



Hair imprints of the gravitational decoupling and hairy black hole spectroscopy

V. F. Guimarães 

*Center for Natural and Human Sciences,
Federal University of ABC, 09210-580, Santo André, Brazil**

R. T. Cavalcanti 

*Institute of Mathematics and Statistics, Rio de Janeiro
State University, 20550-900, Rio de Janeiro, Brazil and
Physics department, São Paulo State University, 12516-410, Guaratingueta, Brazil†*

R. da Rocha 

Center of Mathematics, Federal University of ABC, 09210-580, Santo André, Brazil‡

Hairy black holes by gravitational decoupling (GD) are probed to derive the gravitational waveform produced by perturbation theory applied to these compact objects. Using the Regge–Wheeler and Zerilli equations governing the metric perturbations and applying a higher-order WKB method, the quasinormal modes (QNMs) are computed and discussed. Compared to the QNMs produced in the ringdown phase of Reissner–Nordström black hole solutions, it yields a clear physical signature of primary hair imprinting the hairy GD black hole gravitational waveforms.

* [vitor.guimaraes@ufabc.edu.br](mailto: ritor.guimaraes@ufabc.edu.br)

† [rogerio.cavalcanti@ime.uerj.br](mailto: rogerio.cavalcanti@ime.uerj.br)

‡ [roldao.rocha@ufabc.edu.br](mailto: roldao.rocha@ufabc.edu.br) (corresponding author)

I. INTRODUCTION

Laser-interferometric detection of gravitational waves (GWs) radiated from the final stages of merging binaries has contributed to understanding the strong regime of gravity [1, 2]. This remarkable achievement allows for experimental validation of solutions of the Einstein field equations and their extensions. The gravitational decoupling (GD) technique is a useful and powerful method to derive self-gravitating compact stellar configurations from established solutions in general relativity (GR). This approach naturally leads to the emergence of anisotropic stellar distributions, facilitating the derivation of analytical solutions to the Einstein field equations by incorporating diverse possibilities for the energy-momentum tensor [3, 4]. Within the GD framework, the sources of the GR gravitational field and their corresponding field equations are meticulously split into two disjoint sectors. The first describes the standard GR solution, while the second encompasses additional sources that can embody various forms of charge, ranging from tidal and gauge charges to hairy fields, along with contributions from extended gravity models. A plethora of physically relevant compact stellar configurations derived from the GD method can be found in Refs. [5–14]. Realistic models based on the relativistic description of nuclear interactions also indicate that the interior of stars exhibits anisotropies at extremely high densities. The GD method naturally accommodates pressure anisotropies [15–29]. The GD method can be approached within the gauge/gravity duality, allowing for a comprehensive exploration of physically viable black holes in the infrared limit [30–34]. Additionally, the GD method has been explored and tested by strong deflection limit lensing effects [35]. Ref. [36] introduced the prominent class of hairy GD black holes, which has been broadly applied to relevant theoretical developments [37–46]. Recent studies have also addressed observational aspects of GD hairy black holes. In this context, quasinormal modes (QNMs) emitted from GD hairy solutions, including other important observational aspects, were scrutinized in Refs. [47–55].

Hairy black holes exhibit additional macroscopic degrees of freedom unrelated to quasilocal conserved quantities at the event horizon. How the microscopic description of hairy GD black holes accounts for these extra degrees of freedom representing primary hair suggests an effective approach for deriving analytical solutions. With the first unambiguous observations of GWs by LIGO/Virgo, which directly capture perturbations in the curvature of the spacetime weaving, hairy GD solutions can be thoroughly examined in GW astrophysics. It supports exploring aspects of gravity in the strongly nonlinear regime and assessing any deviations from the predictions of GR. Coalescing binary black hole systems, particularly during the merger ringdown phase, have been

thoroughly analyzed from a direct observational perspective, yielding significant results [56] that may directly provide new insights to hairy GD solutions.

Numerical relativity is an essential tool within the fully nonlinear regime of GR, supporting significant results that also stem from the post-Newtonian regime and black hole perturbation theory. Despite substantial progress, there remain unanswered questions regarding the foundations of GR, such as, e.g., the lack of a complete quantum field theory of gravity and the physical interpretation of gravitational singularities. The range of extensions to GR regarding black hole solutions, associated with the increased sensitivity of future gravitational-wave detectors, may provide an unprecedented opportunity to test the foundational aspects of gravity [57], particularly the hairy GD solutions.

Since the pioneering work of Regge and Wheeler [58], black hole perturbation theory has played a crucial role in exploring the strong field regime of GR [59–61]. With the increasing interest in GWs, black hole perturbation theory and its various applications have become essential tools in gravitational physics [60, 62]. A key setup involves investigating QNMs, which characterize a black hole relaxation process after external perturbations, with several relevant developments in Refs. [63–67]. Perturbation theory also successfully describes binary black hole mergers, during which black holes emit radiation. As the orbital period decreases, the black hole inspirals and merges into a more stable end state through the ringdown phase. Before the rise of numerical relativity, perturbative methods were the most effective means of modeling realistic scenarios in GR in the nonlinear regime. QNMs describe energy dissipation from fields in a black hole background and can be formally derived from linearized differential equations of GR that constrain perturbations around a black hole solution. QNMs calculated within the linearized framework align closely with those derived from a nonlinear, coupled system of Einstein’s equations, particularly for late times [68–71].

Quasinormal ringing plays a dominant role in phenomena related to black hole perturbations and provides distinct signatures that enable the clear observational identification of hairy GD black holes. To extract substantial information from GW detectors, it is essential to thoroughly understand the main features and signatures of QNMs associated with a hairy GD black hole, whose event horizon behaves as a membrane for classical fields, resulting in a non-Hermitian boundary value problem with complex eigenmodes [72, 73]. The imaginary part of the frequency captures the decay timescale of the black hole perturbation and quantifies the energy lost by the black hole. Perturbed black holes are inherently dissipative due to the effects of the event horizon. These modes dominate the radiation emitted during the intermediate stages of black hole perturbation

[74]. QNMs have a specific dependence on the black hole parameters, making them valuable tools for comparing theoretical predictions with observational data. In this context, the spectrum of hairy GD black holes can unveil possible observational signatures indicative of the GD setup. Therefore, the main aim of this work is to derive the QN spectrum of frequencies for hairy GD black hole solutions and analyze the resulting deviations from the standard Schwarzschild solution, as the GD hairy parameters are introduced. We will derive the complex frequencies at which black holes oscillate and at which their GWs propagate. These QNMs contain not only characteristic information about the black hole that emitted them, regarding their no-hair charges, and may also encode primary hair signatures that could be observed in GW detections. We will study the spectra of the QNMs from hairy GD potentials, searching for hair signatures that allow one to distinguish a hairy black hole solution from those satisfying the no-hair conjectures.

In this work, the GD is implemented for splitting gravitational sources, generating new terms in the metric that are interpreted as primary hair. We apply perturbation theory to investigate the form and properties of the GWs produced by hairy GD black hole solutions through the analysis of their QNMs. From the Regge–Wheeler and Zerilli equations governing the metric perturbation, which applies a higher-order WKB method, QNMs are obtained and analyzed. We also implement the same method to obtain the QNMs for a Reissner–Nordström (RN) black hole with the same values of the outer horizon and square of the charge for each of the three hairy black hole metrics obtained by the GD method, to analyze and quantify their distinctiveness, which could be considered a primary hair signature in the QNMs of GD hairy black hole GWs.

This paper is organized as follows: Section II is dedicated to reviewing the GD procedure and its main results, leading to GD hairy black hole solutions after some constraints are imposed, which are the focus of Section III. In Section IV, we briefly discuss black hole perturbation theory for curved backgrounds and investigate its results when applied to the GD metrics, i.e., the hairy black hole odd potentials. Next, in Section V we present and analyze the quasi-normal modes, obtained via sixth-order WKB method, from the GD hairy black hole odd potentials and compare the resulting spectrum with one obtained by the same method when applied to a no-hair solution with the same outer horizon and squared charge values. Section V is devoted to computing the complex frequency differences $\Delta\omega$ between these spectra and analyzing their significance with respect to the error of the WKB method at sixth-order. Conclusions are presented in Section VI.

II. GRAVITATIONAL DECOUPLING

The GD method stems from another procedure known as the minimal geometric deformation (MGD) [3], developed to obtain braneworld configurations from general relativistic perfect fluid solutions and conversely [75]. In the context of the MGD, 4-dimensional GR solutions can be derived when terms containing the electric part of the Weyl tensor field and a second-order combination of the energy-momentum tensor are regarded on the right-hand side of Einstein field equations. These solutions can manifest anisotropy. In the membrane paradigm of AdS/CFT the additional tensor field, implementing the GD protocol, would contain all the higher-dimensional contributions to the resulting curved geometry through the Weyl tensor field, as Kaluza–Klein modes and moduli fields [33, 35, 76–78]. However, even without higher-dimensional scenarios, the 4-dimensional GD apparatus can promote and accommodate eventual effects of dark matter, dark energy, fields beyond baryonic matter, quantum corrections, and other quantum gravity effects.

To implement the GD, the Einstein field equations

$$G_{\mu\nu} = 8\pi\check{T}_{\mu\nu} \quad (1)$$

are taken into account, where a new energy-momentum tensor $\check{T}_{\mu\nu}$ is defined as a combination of two other energy-momentum tensors as

$$\check{T}_{\mu\nu} \equiv T_{\mu\nu} + \alpha\theta_{\mu\nu}, \quad (2)$$

where $T_{\mu\nu}$ is the usual energy-momentum tensor representing baryonic matter (in this case, a perfect fluid), and $\theta_{\mu\nu}$ is an extra tensor field coupled to $T_{\mu\nu}$. The tensor field $\theta_{\mu\nu}$ represents a second independent gravitational sector, which is related to the primary gravitational sector by the coupling constant α and the following conservation equation [3, 36]:

$$\nabla^\mu (T_{\mu\nu} + \alpha\theta_{\mu\nu}) = \nabla^\mu \check{T}_{\mu\nu} = 0. \quad (3)$$

In the case where the seed geometry is described by the usual spherically symmetric line element

$$ds_{\text{seed}}^2 = -e^{\xi(r)} dt^2 + e^{\mu(r)} dr^2 + r^2 d\Omega^2, \quad (4)$$

Eq. (1) then yields

$$8\pi (T_0^0 + \alpha\theta_0^0) = - (r\mu' + e^\mu - 1) \frac{e^{-\mu}}{r^2}, \quad (5a)$$

$$8\pi (T_1^1 + \alpha\theta_1^1) = - (r\xi' - e^\mu + 1) \frac{e^{-\mu}}{r^2}, \quad (5b)$$

$$8\pi (T_2^2 + \alpha\theta_2^2) = \left[r (\xi')^2 - (r\mu' - 2)\xi' + 2r\xi'' - 2\mu' \right] \frac{e^{-\mu}}{4r}. \quad (5c)$$

The first thing to notice is that by setting the effective energy density, the radial pressure, and the tangential pressures as

$$\check{\rho} \equiv T_0^0 + \alpha\theta_0^0, \quad (6)$$

$$\check{p}_r \equiv -T_1^1 - \alpha\theta_1^1, \quad (7)$$

$$\check{p}_t \equiv -T_2^2 - \alpha\theta_2^2, \quad (8)$$

while assuming $T_{\mu\nu}$ is a perfect fluid, i.e.,

$$T_0^0 = \rho, \quad T_1^1 = -p, \quad T_2^2 = -p, \quad (9)$$

then Eqs. (5a) – (5c), along with Eq. (9), yields

$$\Pi = \check{p}_r - \check{p}_t \neq 0, \quad (10)$$

where ρ and p are the perfect fluid energy density and isotropic pressure, respectively. Thus, as seen in Eq. (10), a relevant attribute of the GD is the ability to generate GR solutions for anisotropic fluid configurations [3, 79]. It is important to remember that the existence of the anisotropy (10) is directly related to the presence of the second gravitational sector implemented by the $\theta_{\mu\nu}$ tensor field.

One could naively try to take Eqs. (5a) – (5c) and separate their sources, constructing two sets of equations, one for $\theta_{\mu\nu}$ and one for $T_{\mu\nu}$. However, the high non-linearity of Eq. (1) forbids it [3]. To circumvent this issue, the seed spacetime geometry is modified by the presence of the second gravitational sector. One can show that for a given additional Lagrangian density, \mathcal{L}_θ associated with $\theta_{\mu\nu}$, the complete action reads:

$$\hat{S} = \frac{1}{16\pi} S_H + S_M + S_\theta \quad (11)$$

$$= \int \left(\frac{1}{16\pi} R + \mathcal{L}_M + \mathcal{L}_\theta \right) \sqrt{-g} \, d^4x, \quad (12)$$

where S_H , S_M and S_θ are the Einstein-Hilbert action and the actions regarding the first and second gravitational sectors, respectively. Defining $\theta_{\mu\nu}$ as [3, 36]

$$\frac{2}{\sqrt{-g}} \frac{\delta(\sqrt{-g}\mathcal{L}_\theta)}{\delta g^{\mu\nu}} = 2 \frac{\delta\mathcal{L}_\theta}{\delta g^{\mu\nu}} - g_{\mu\nu}\mathcal{L}_\theta \equiv \theta_{\mu\nu}, \quad (13)$$

the resulting geometry is deformed away from the seed solution, which is simply Eq. (1) with $\alpha = 0$ [36]:

$$\xi(r) \mapsto \nu(r) = \xi(r) + \alpha\sigma(r), \quad (14)$$

$$e^{-\mu(r)} \mapsto e^{-\lambda(r)} = e^{-\mu(r)} + \alpha\kappa(r), \quad (15)$$

where $\sigma(r)$ and $\kappa(r)$ are the geometric deformation functions [36]. For a spherically symmetric seed solution, the above deformation yields:

$$\begin{aligned} ds^2 &= -e^{\nu(r)} dt^2 + e^{\lambda(r)} dr^2 + r^2 d\Omega^2, \\ &= -e^{[\xi(r) + \alpha\sigma(r)]} dt^2 + \frac{1}{e^{-\mu(r)} + \alpha\kappa(r)} dr^2 + r^2 d\Omega^2. \end{aligned} \quad (16)$$

Note that the $\alpha \rightarrow 0$ limits yields $e^{\nu(r)} \mapsto e^{\xi(r)}$ and $e^{\lambda(r)} \mapsto e^{\mu(r)}$, implying that $ds^2 \mapsto ds_{\text{seed}}^2$.

Plugging Eq. (16) into Eq. (1) produces the set of equations

$$8\pi T_0^0 = -\left(r\mu' + e^\mu - 1\right) \frac{e^{-\mu}}{r^2}, \quad (17a)$$

$$8\pi T_1^1 = -\left(r\xi' - e^\mu + 1\right) \frac{e^{-\mu}}{r^2}, \quad (17b)$$

$$8\pi T_2^2 = \left[r(\xi')^2 - (r\mu' - 2)\xi' + 2r\xi'' - 2\mu'\right] \frac{e^{-\mu}}{4r}, \quad (17c)$$

at the zeroth order in α , i.e., regarding the seed metric and also the set of equations

$$8\pi\alpha\theta_0^0 = \frac{\alpha}{r^2}(r\kappa' + \kappa), \quad (18a)$$

$$8\pi\alpha\theta_1^1 + \alpha Z_1 = -\frac{\alpha\kappa}{r^2}(1 + r\nu'), \quad (18b)$$

$$8\pi\alpha\theta_2^2 + \alpha Z_2 = -\alpha\frac{\kappa}{4}\left(2\nu'' + (\nu')^2 + \frac{2\nu'}{r}\right) - \alpha\frac{\kappa'}{4}\left(\nu' + \frac{2}{r}\right), \quad (18c)$$

up to $\mathcal{O}(\alpha^2)$, related to the second gravitational sector, known as quasi-Einstein equations [36], where

$$Z_1 = \frac{e^{-\mu}\sigma'}{r}, \quad (19)$$

$$Z_2 = \frac{e^{-\mu}}{4}\left(2\sigma'' + (\sigma')^2 + \frac{2\sigma'}{r} + 2\xi'\sigma' - \mu'\sigma'\right). \quad (20)$$

Therefore, two sets of equations are obtained, one for each gravitational sector. However, the $\theta_{\mu\nu}$ and $T_{\mu\nu}$ tensors are also related by the conservation equation. Thus, to complete the decoupling

process, one must set

$$\nabla^{(\text{def})}_{\mu} \check{T}^{\mu}_{\nu} = 0, \quad (21)$$

which states that the deformed Einstein tensor field must satisfy its own Bianchi identity, where $\nabla^{(\text{def})}$ is the covariant derivative compatible with the deformed metric (16). Developing Eq. (21) yields

$$\nabla^{(\text{def})}_{\mu} \check{T}^{\mu}_{\nu} = \nabla^{(\text{def})}_{\mu} (T^{\mu}_{\nu} + \theta^{\mu}_{\nu}). \quad (22)$$

The Bianchi identity from the seed geometry yields

$$\nabla^{(\text{seed})}_{\mu} T^{\mu}_{\nu} = 0, \quad (23)$$

where $\nabla^{(\text{seed})}$ is the covariant derivative compatible to ds_{seed}^2 . Eq (23) explicitly reads

$$-\frac{1}{2} \left(T_{00} \xi' - T_{11} \xi' - \frac{4 T_{11}}{r} + \frac{4 T_{22}}{r} - 2 T'_{11} \right) e^{-\mu} = 0. \quad (24)$$

From Eq. (22), one concludes that

$$\begin{aligned} \nabla^{(\text{def})}_{\mu} T^{\mu}_{\nu} &= -\frac{\alpha \sigma'}{2} (T_{00} - T_{11}) e^{-\lambda} + \left(T_{00} \xi' - T_{11} \xi' - \frac{4 T_{11}}{r} + \frac{4 T_{22}}{r} - 2 T'_{11} \right) e^{-\lambda} \\ &= -\frac{\alpha \sigma'}{2} (T_{00} - T_{11}) e^{-\lambda} + \nabla^{(\text{seed})}_{\mu} T^{\mu}_{\nu} \\ &= -\frac{\alpha \sigma'}{2} (T_{00} - T_{11}) e^{-\lambda}. \end{aligned} \quad (25)$$

Identifying the second line of Eq. (25) as the left-hand side (LHS) of Eq. (24), substituting it back into Eq. (22) yields

$$\nabla^{(\text{def})}_{\mu} \check{T}^{\mu}_{\nu} = \nabla^{(\text{def})}_{\mu} \theta^{\mu}_{\nu} - \frac{\alpha \sigma'}{2} (T_{00} - T_{11}) e^{-\lambda}. \quad (26)$$

Therefore, for the complete system and its two gravitational sectors to conserve energy-momentum, one must require that:

$$\nabla^{(\text{def})}_{\mu} \theta^{\mu}_{\nu} = \frac{\alpha \sigma'}{2} (T_{00} - T_{11}) e^{-\lambda}. \quad (27)$$

It implies that either $\theta_{\mu\nu}$ and $T_{\mu\nu}$ must exchange energy-momentum or one of the following two options must be satisfied:

$$T_{00} = T_{11}, \quad (28a)$$

$$T_{\mu\nu} = 0, \quad (28b)$$

i.e., if $T_{\mu\nu}$ satisfies the equation of state (28a), or if the first gravitational sector corresponds to vacuum (28b), then the energy-momentum exchange is not necessary, since the term $\nabla^{(\text{def})}_{\mu}\tilde{T}^{\mu}_{\nu}$ would trivially go to zero. Satisfying any of these options gives us a complete decoupling of the gravitational sectors represented by $\theta_{\mu\nu}$ and $T_{\mu\nu}$. To decouple the gravitational system, the first step is to take Eqs. (17a) – (17c), along with $\nabla^{(\text{seed})}_{\mu}T^{\mu\nu} = 0$, and solve them for $\{\mu, \xi, \rho, p\}$. Equipped with the equation of state for $\theta_{\mu\nu}$ and Eq. (27), one must simply substitute $\{\mu, \xi, \rho, p\}$ into Eqs. (18c), and solve for $\{\kappa, \sigma, \theta_{00}, \theta_{11}, \theta_{22}\}$.

Assuming that the seed metric is a black hole solution, such as the Schwarzschild spacetime, one must impose constraints to make sure that the deformed solution is still a black hole, and the consequences will finally lead us to the uncovering of the hairy charges that will later be identified as hair [36].

III. HAIRY BLACK HOLES BY GD

From now on, we will work in the context of a Schwarzschild seed spacetime in a tensor-vacuum [36], as in 28b, which is achieved by setting $T_{\mu\nu} = 0$, leaving a spherically symmetric source $\theta_{\mu\nu}$ as the only energy-momentum tensor present, which will induce the metric deformation. Then, as suggested by Eq. (16), the line element becomes [36]:

$$ds^2 = - \left(1 - \frac{2M}{r}\right) e^{\alpha\sigma(r)} dt^2 + \left(1 - \frac{2M}{r} + \alpha\kappa(r)\right)^{-1} dr^2 + r^2 d\Omega^2, \quad (29)$$

which is the same as applying the GD method to a seed Schwarzschild spacetime. As seen in Ref. [36], to avoid pathological metric signatures, a black hole solution must have the event horizon coincide with Killing horizons, i.e.:

$$e^{\nu(r_h)} = 0 = e^{-\lambda(r_h)}, \quad (30)$$

where $r = r_h$ is the point that hosts both horizons. Thus, setting:

$$e^{\nu(r)} = f(r) = e^{-\lambda(r)}, \quad (31)$$

where $f(r)$ is a generic, static metric function, along with the causal condition in Eq. (30), i.e., $f(r_h) = 0$, entails the following relation between the geometric deformation functions [36]:

$$\left(1 - \frac{2M}{r}\right) \left(e^{\alpha\sigma(r)} - 1\right) = \alpha\kappa(r), \quad (32)$$

which implies:

$$f(r) = \left(1 - \frac{2M}{r}\right) e^{\alpha\sigma(r)}, \quad (33)$$

consequently, turning

$$ds^2 = -f(r) dt^2 + f(r)^{-1} dr^2 + r^2 d\Omega^2 \quad (34)$$

into:

$$ds^2 = -\left(1 - \frac{2M}{r}\right) e^{\alpha\sigma(r)} dt^2 + \frac{dr^2}{\left(1 - \frac{2M}{r}\right) e^{\alpha\sigma(r)}} + r^2 d\Omega^2. \quad (35)$$

As just demonstrated, imposing a well-behaved causal structure yields a direct relation between the deformation functions $\{\sigma, \kappa\}$, thus reducing the number of unknown quantities, which now are $\{\sigma(r), \theta_0^0, \theta_1^1, \theta_2^2\}$. As mentioned before, along with the quasi-Einstein equations (18a) – (18c) and (27), an equation of state is needed for $\theta_{\mu\nu}$ to completely solve this system. Let us analyze the case where $\theta_{\mu\nu}$ satisfies the dominant energy condition (DEC), implying:

$$\check{\rho} \geq |\check{p}_r|, \quad (36a)$$

$$\check{\rho} \geq |\check{p}_t|. \quad (36b)$$

Eq. (30) therefore infers that $\check{\rho}(r) = -\check{p}_r(r)$. Using the definitions of the effective pressures and effective density, and saturating Eq. (36a), then Eqs. (36) turns into:

$$-\theta_0^0 + \theta_2^2 \leq 0, \quad (37a)$$

$$-\theta_0^0 - \theta_2^2 \leq 0. \quad (37b)$$

Plugging the expressions for the tensor field components given by the quasi-Einstein field equations, Eqs. (37) become:

$$r(r - 2M)(e^{\alpha\sigma})'' + 4(r - M)(e^{\alpha\sigma})' + 2(e^{\alpha\sigma}) + 2 \leq 0, \quad (38)$$

$$r(r - 2M)(e^{\alpha\sigma})'' + 4M(e^{\alpha\sigma})' - 2(e^{\alpha\sigma}) + 2 \geq 0. \quad (39)$$

Saturating Eqs. (38) and (39) and solving each of them yields the Reissner-Nordström (RN) and Schwarzschild-de Sitter solutions, respectively. Saturating both Eqs. (38) and (39) implies that the $\theta_{\mu\nu} = 0$, which trivially leads to the Schwarzschild spacetime. To see what happens to the

non-saturated inequalities, let us impose the LHS of both Eqs. (38) and (39) must equal zero near the event horizon and far from the source. Proposing a simple function,

$$G(r) \equiv \alpha \left(\frac{r}{M} - 2 \right) e^{-\frac{r}{M}}, \quad (40)$$

such that $G(r) = 0$ for both the ranges $r \sim 2M$ and $r \gg M$, setting Eq. (38) equal to $G(r)$, and solving for $e^{\alpha\sigma(r)}$, one obtains [36]:

$$e^{\alpha\sigma(r)} = 1 - \frac{1}{(r-2M)} \left[\alpha \left(\ell + M e^{-r/M} \right) - \frac{Q^2}{r} \right]. \quad (41)$$

The constants of integration have been re-labeled in such a way as to ensure that the Schwarzschild spacetime can be recovered in the limit $\alpha \rightarrow 0$. The reasons behind this choice of labels become evident when one substitutes $e^{\alpha\sigma(r)}$ back in Eq. (33), such that $f(r)$ becomes [36]:

$$f_{\text{GD}}(r) = 1 - \frac{2\mathcal{M}}{r} + \frac{Q^2}{r^2} - \alpha \frac{M}{r} e^{-r/M}, \quad (42)$$

where a re-scaled mass $2\mathcal{M} = 2M + \alpha\ell$ is introduced. As can be seen, the metric function $f_{\text{GD}}(r)$ (42) has the same form as $f_{\text{RN}}(r)$, the RN metric function [80], apart from the $e^{-r/M}$ term. It is important to highlight that the dimensionality and the interpretation of the constant Q in $f_{\text{GD}}(r)$ are distinct from the RN counterpart to the hairy GD black hole solutions. In the RN spacetime, Q is the electric charge that fuels the black hole electromagnetic field, whereas in Eq. (42), Q is proportional to α and has dimensions of length, as does ℓ [36]. However, it can be said that both the electromagnetic energy-momentum tensor $E_{\mu\nu}$ and $\theta_{\mu\nu}$ play analogous roles in their respective scenarios, since they both are the agents that deform the seed geometry away from the Schwarzschild solution. As a matter of fact, in Ref. [4] the tensor $\theta_{\mu\nu}$ is substituted by $E_{\mu\nu}$ to show the effectiveness of the GD method in solving the Einstein field equations and arriving at the RN solution by decoupling the Einstein-Maxwell system.

Due to Eq.(42), the resulting line element of Eq. (34) yields [36]:

$$ds^2 = - \left(1 - \frac{2\mathcal{M}}{r} + \frac{Q^2}{r^2} - \alpha \frac{M}{r} e^{-r/M} \right) dt^2 + \left(1 - \frac{2\mathcal{M}}{r} + \frac{Q^2}{r^2} - \alpha \frac{M}{r} e^{-r/M} \right)^{-1} dr^2 + r^2 d\Omega^2. \quad (43)$$

This solution, for $r \gg M$, goes to an RN solution, as the fourth and extra $1/r$ term in the metric functions falls exponentially with increasing quotient r/M . The charges $\{\ell, Q\}$ are thus considered to be possible generators of primary hair [36], which makes Eq. (43) a hairy black hole solution of the Einstein field equations.

For Eq. (39) to be satisfied, the following constraint must be imposed:

$$Q^2 \geq \frac{r^2 \alpha}{4M} (r + 2M) e^{-\frac{r}{M}}. \quad (44)$$

The line element (43), along with the definitions for the effective pressures and energy density, informs that this deformed geometry is generated by:

$$\check{\rho} = \frac{Q^2}{8\pi r^4} - \frac{\alpha e^{-\frac{r}{M}}}{8\pi r^2}, \quad (45)$$

$$\check{p}_r = -\frac{Q^2}{8\pi r^4} + \frac{\alpha e^{-\frac{r}{M}}}{8\pi r^2} = -\check{\rho}, \quad (46)$$

$$\check{p}_t = \frac{Q^2}{8\pi r^4} - \frac{\alpha e^{-r/M}}{16\pi M r}. \quad (47)$$

Plugging Eqs. (45) – (47) into the DEC constraint $\check{\rho} \geq |\check{p}_t|$, and simplifying, yields $r \geq 2M$. Hence, in this case, satisfying the DEC ultimately means satisfying $r \geq 2M$. Furthermore, analyzing the line element (42) at the horizon $r = r_h$ shows that:

$$1 - \frac{2M + \alpha\ell}{r_h} + \frac{Q^2}{r_h^2} - \frac{\alpha M e^{-\frac{r_h}{M}}}{r_h} = 0, \quad (48)$$

which means that there will be two horizons: an inner r_- and an outer r_+ horizon, also known as the Cauchy and event horizons, respectively, solutions of the following quadratic equation:

$$r_h^2 = -Q^2 + r_h \left(2M + \alpha\ell + \alpha M e^{-\frac{r_h}{M}} \right). \quad (49)$$

Eq. (44) for $r \geq 2M$, reads:

$$Q^2 \geq \frac{4\alpha M^2}{e^2}, \quad (50)$$

which in turn, due to (49), yields:

$$\ell \geq \frac{M}{e^2}, \quad (51)$$

illustrating the full outspread of the DEC. However, solving Eq. (49) is not an easy task. Three possible analytical solutions are immediate for the following values of Q^2 :

$$Q^2 = \frac{4\alpha M^2}{e^2}, \quad (52a)$$

$$Q^2 = r_+ \left(2M + \alpha M e^{-\frac{r_+}{M}} \right), \quad (52b)$$

$$Q^2 = \alpha r_+ M e^{-\frac{r_+}{M}}. \quad (52c)$$

These values, through Eq. (49), will yield r_+ equal to $2M$, $\alpha\ell$ and $2M + \alpha\ell$, respectively. To simplify equations, one may set $r_+ = \beta M$, with $\beta \geq 2$, which, along with the Eqs. (52a) – (52c), allows to make $M = M(Q)$, turning $f_{\text{GD}}(r)$ into:

$$f_{\text{GD}}(r) = 1 - \frac{2M}{r} + \frac{Q^2}{r^2} - \frac{(\alpha/\beta)r_+}{r} e^{-\beta r/r_+}. \quad (53)$$

Eq. (53) can be thought of as a master equation, which generates, for each of the three possible pairs $\{r_+, Q\}$, a deformed metric function, presented next in explicit forms:

$$f_{GD_1}(r) = 1 - \frac{2\mathcal{M}}{r} + \frac{Q^2}{r^2} - \frac{Q\sqrt{\alpha}e^{\left(-\frac{2r\sqrt{\alpha}}{eQ}+1\right)}}{2r}, \quad (54)$$

$$f_{GD_2}(r) = 1 - \frac{2\mathcal{M}}{r} + \frac{Q^2}{r^2} - \frac{Q\alpha e^{\left(-\frac{r}{Q}\sqrt{\frac{(2e^{\ell_0}+\alpha)\ell_0}{e^{\ell_0}}}\right)}}{\sqrt{\alpha\ell_0 e^{(-\ell_0)} + 2\ell_0}r}, \quad (55)$$

$$f_{GD_3}(r) = 1 - \frac{2\mathcal{M}}{r} + \frac{Q^2}{r^2} - \frac{Q\alpha e^{\left(-\frac{r}{Q}\sqrt{\frac{\alpha(\ell_0+2)}{e^{\ell_0+2}}} + \frac{1}{2}\ell_0+1\right)}}{\sqrt{\alpha\ell_0 + 2\alpha}r}, \quad (56)$$

where $\ell_0 = \alpha\ell$. Applying the following transformation

$$\bar{\mathcal{M}} = \vartheta\mathcal{M}, \quad (57)$$

$$\bar{Q}^2 = \vartheta Q^2, \quad (58)$$

where

$$\vartheta \equiv \left(1 - \frac{\alpha e^{-\beta}}{\beta}\right)^{-1}, \quad (59)$$

the expression for r_+ takes the familiar form:

$$r_+ = \bar{\mathcal{M}} + \sqrt{\bar{\mathcal{M}}^2 - \bar{Q}^2}, \quad (60)$$

which reproduces the form that r_+ takes in the RN geometry [36, 80]. It leads to the conclusion that assuming Q to be an electric charge, then it must match a non-linear electrodynamics, with an associated Lagrangian through the P-dual formalism as obtained in Ref. [36]. However, it is important to remember that, a priori, $Q^2 \propto \alpha$, which has the dimension of length and allows us to recover the Schwarzschild spacetime for $\alpha \rightarrow 0$, as expected.

The quasi-RN nature of the deformed metric functions (54) – (56) gives rise to the question of how similar their gravitational wave (GW) signatures are, concerning those from an RN black hole with the same values for Q^2 . In the next section, we address these questions by computing the QNMs of the deformed metrics and RN black holes with the same Q^2 and equivalent mass, so that we can look for possible signatures that would allow us to unequivocally distinguish them in terms of the gravitational waveform.

IV. GRAVITATIONAL WAVES FROM HAIRY BLACK HOLES

A. Perturbations in curved backgrounds

Einstein predicted GWs through a linearized version of GR, an approach that imposes the decomposition of the metric as

$$g_{\mu\nu} = \dot{g}_{\mu\nu} + h_{\mu\nu}, \quad |h_{\mu\nu}| \ll \dot{g}_{\mu\nu}, \quad (61)$$

where $\dot{g}_{\mu\nu}$ is the background spacetime and $h_{\mu\nu}$ is a perturbation maintained small enough by the right choice of gauge provided by GR invariance under infinitesimal diffeomorphisms [72, 81, 82].

Black hole perturbation theory states that, in the context of curved backgrounds, the perturbed Ricci tensor is given by the Palatini identity [72, 82]:

$$\delta R_{\mu\nu} = \frac{1}{2} (\nabla_\sigma \nabla_\mu h_\nu^\sigma + \nabla_\sigma \nabla_\nu h_\mu^\sigma - \nabla^\sigma \nabla_\sigma h_{\mu\nu} - \nabla_\nu \nabla_\mu h), \quad (62)$$

which yields the perturbed Einstein tensor:

$$\delta G_{\mu\nu} \equiv \delta R_{\mu\nu} - \frac{1}{2} \dot{g}_{\mu\nu} \left(\dot{g}^{\alpha\beta} \delta R_{\alpha\beta} - h^{\alpha\beta} \dot{R}_{\alpha\beta} \right) - \frac{1}{2} h_{\mu\nu} \dot{R}. \quad (63)$$

The previous section presented the GD background with a $1/r^2$ dependency, alike the RN geometry. Hence, to obtain the wavelike equations that govern the GWs emitted from hairy GD solutions, one may implement the procedure due to Regge–Wheeler [58] and Zerilli [83]. Such a procedure involves performing a harmonic decomposition of the spacetime manifold, decomposing the perturbation tensor, and consequently the perturbed Einstein tensor [72, 82]. Thereafter, one can rewrite them in terms of spherical tensors to take advantage of the spherical symmetry and easily separate the angular from the radial parts by the orthogonality relations. The radial parts may be separated with respect to parity, rendering two sets of Einstein equations: odd and even. Each set, after some manipulation, yields a Schrödinger-like equation known as the Regge–Wheeler and Zerilli master equations for the odd and even perturbations, respectively [83]. In this section, we will focus on the odd perturbations of the hairy GD black hole solutions.

The perturbation tensor $h_{\mu\nu}$ may be decomposed with respect to parity as such:

$$h_{\mu\nu}(t, r, \theta, \phi) = \sum_{m,n} \int_{-\infty}^{+\infty} \tilde{h}_{\mu\nu}^{mn}(\omega, r, \theta, \phi) e^{-i\omega t} d\omega = \sum_{m,n} \int_{-\infty}^{+\infty} \left(\tilde{h}_{\mu\nu}^{e,mn} + \tilde{h}_{\mu\nu}^{o,mn} \right) e^{-i\omega t} d\omega, \quad (64)$$

where a Fourier transform was also performed, due to the static character of the hairy GD black hole solutions, and where $\tilde{h}_{\mu\nu}^{e,mn}$ and $\tilde{h}_{\mu\nu}^{o,mn}$ are the even and odd perturbations, respectively. Their explicit form is given below in terms of scalar and vector spherical harmonics $\{e_a^{o,mn}, Y^{mn}\}$, as

well as the blackening factor $f = f(r)$, the odd $\{\tilde{h}_0^{o,mn}, \tilde{h}_1^{o,mn}\}$, and even perturbation functions $\{\tilde{h}_0^{mn}, \tilde{h}_1^{mn}, \tilde{h}_2^{mn}, \tilde{K}^{mn}\}$:

$$\tilde{h}_{\mu\nu}^{o,mn} = \begin{pmatrix} 0 & 0 & \tilde{h}_0^{o,mn} e_\theta^{o,mn} & \tilde{h}_0^{o,mn} e_\phi^{o,mn} \\ 0 & 0 & \tilde{h}_1^{o,mn} e_\theta^{o,mn} & \tilde{h}_1^{o,mn} e_\phi^{o,mn} \\ * & * & 0 & 0 \\ * & * & 0 & 0 \end{pmatrix}, \quad (65)$$

$$\tilde{h}_{\mu\nu}^{e,mn} = \begin{pmatrix} f\tilde{h}_0^{mn} & \tilde{h}_1^{mn} & 0 & 0 \\ \tilde{h}_1^{mn} & f^{-1}\tilde{h}_2^{mn} & 0 & 0 \\ 0 & 0 & r^2\tilde{K}^{mn} & 0 \\ 0 & 0 & 0 & r^2\sin^2\theta\tilde{K}^{mn} \end{pmatrix} Y^{mn}. \quad (66)$$

The three aforementioned odd equations

$$\tilde{\beta}_0^{mn}(\omega, r) = f(\tilde{h}_{0,mn}'' + i\omega\tilde{h}_{1,mn}') - 2i\omega\frac{f}{r}\tilde{h}_1^{mn} + \left[\frac{f''}{2} + \frac{n(n+1) + f - 1}{r^2}\right]\tilde{h}_0^{mn}, \quad (67a)$$

$$\tilde{\beta}_1^{mn}(\omega, r) = \frac{i\omega}{rf}(r\tilde{h}_{0,mn}' - 2\tilde{h}_0^{mn}) + \left[\frac{f''}{2} - \frac{\omega^2}{f} + \frac{(n(n+1) - f - 1)}{r^2}\right]\tilde{h}_1^{mn}, \quad (67b)$$

$$\tilde{t}_{mn}(\omega, r) = i\omega f^{-1}\tilde{h}_0^{mn} + f\tilde{h}_{1,mn}' + f'\tilde{h}_1^{mn}, \quad (67c)$$

extracted from the odd Einstein tensor components, when properly manipulated, yield the Regge–Wheeler master equation:

$$\frac{d^2 Q_{mn}}{dr_*^2} + (\omega^2 - \hat{V}_{mn}^{\text{odd}}) Q_{mn} = S_{mn}^{\text{odd}}, \quad (68)$$

where S_{mn}^{odd} is the source term, $Q_{mn} \equiv f\tilde{h}_1^{mn}/r$ is the Regge–Wheeler function, r_* is the tortoise coordinate related to r by the equation:

$$dr_* = \frac{1}{f} dr, \quad (69)$$

and finally, $\hat{V}_{mn}^{\text{odd}}$ is the Regge–Wheeler potential, which governs the behavior of the odd perturbations, constructed according to the version of the Regge–Wheeler equation developed in Ref. [83] for the RN background:

$$\hat{V}_{mn}^{\text{odd}} = \frac{f}{r^2} \left[\frac{1}{2} r^2 f'' - r f' + n(n+1) + f - 1 - \frac{2Q^2}{r^2} \right]. \quad (70)$$

By substituting the blackening factor f for the GD metric functions (54), (55), and (56), we obtain the three odd GD potentials V_{GD_1} , V_{GD_2} and V_{GD_3} , respectively. These potentials will be

the source of the QNMs to be computed and analyzed in the next section. Now, let us further analyze the GD metric functions and the corresponding odd potentials they span through Eq. (70).

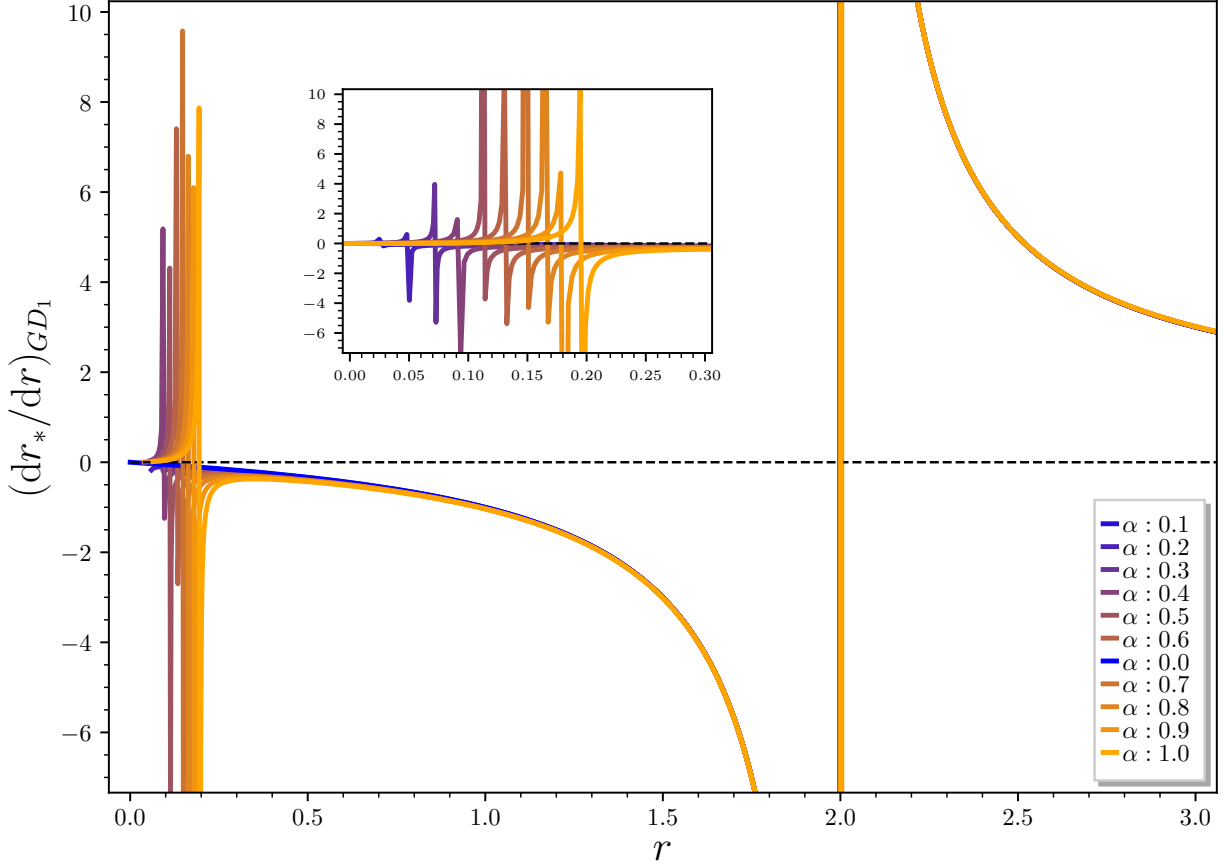


FIG. 1: Behavior of $(dr_*/dr)_{GD1} = f_{GD1}^{-1}$ as a function of r for different values of α , in units of M , and $n = 2$. The event horizon lies at $r = 2$, but the Cauchy horizon assumes larger values for larger α .

B. Hairy black hole odd potentials

The metric functions of Eqs. (54), (55), and (56) may be rewritten in the following, more convenient form:

$$f_{GD1}(r) = 1 - \frac{(2 + \alpha\ell + \alpha e^{-r})}{r} + \frac{4\alpha e^{-2}}{r^2} \quad (r_+ = 2) \quad , \quad (71a)$$

$$f_{GD2}(r) = 1 - \frac{(2 + \alpha\ell + \alpha e^{-r})}{r} + \frac{\alpha\ell(2 + \alpha e^{-\alpha\ell})}{r^2} \quad (r_+ = \alpha\ell) \quad , \quad (71b)$$

$$f_{GD3}(r) = 1 - \frac{(2 + \alpha\ell + \alpha e^{-r})}{r} + \frac{\alpha(2 + \alpha\ell)e^{-\alpha\ell-2}}{r^2} \quad (r_+ = 2 + \alpha\ell) \quad , \quad (71c)$$

where we substituted the corresponding values for Q^2 from Eqs. (52a), (52b), and (52c), respectively, and set $M = 1$. For the rest of the discussion, we set $r_+ = 3$ for f_{GD_2} and f_{GD_3} , such that they satisfy the DEC.

In Figs. 1 – 3, we see that r_h indeed assumes two values in all three potentials. In these plots, the outer horizons r_+ are fixed either at $r = 2$ or $r = 3$, in units of M , for all values of α , while the inner horizons r_- assume different values for different α . In Fig. 1 we see that, for $\alpha > 0$, the metric functions follow the behavior of the Schwarzschild solution, here represented by the $\alpha = 0$ line. However, as we approach $r = 0$ from the right, the metric functions for $\alpha > 0$ deviate from $\alpha = 0$, and it becomes clear that the values for r_- grow with increasing α , approaching $r_+ = 2$.

As seen in Fig. 2, for every $\alpha > 0$, the metric function f_{GD_2} reproduces the behavior of the usual Schwarzschild blackening factor f_{Schw} , asymptotically, but deviates from it as one approaches $r = 0$ from $+\infty$, alike the previous case. However, in contrast to f_{GD_1} , in this case the values for r_- decrease with increasing α , making the inner horizons increasingly distant from r_+ , here fixed at $r = 3$. As for f_{GD_3} , its behavior is very similar to f_{GD_2} , the key difference is, again, the response of the inner horizons. The event horizon is again fixed at $r = 3$, but the values of r_- grow with increasing α , approaching outer and inner horizons, as it did for f_{GD_1} .

As previously mentioned, the $1/r^2$ terms indicate that we must use the Regge–Wheeler equation developed for RN spacetimes to appropriately understand the odd perturbations for the hairy black hole solutions. Thus, plugging the deformed metric functions into Eq. (70) we obtain the full GD potentials, as seen in Figs. 4 – 6, where it is also possible to see that for $\alpha \rightarrow 0$, all three potentials $\{V_{\text{GD}_1}, V_{\text{GD}_2}, V_{\text{GD}_3}\}$ become

$$V = \left(1 - \frac{2}{r}\right) \left(\frac{n(n+1)}{r^2} - \frac{6}{r^3}\right), \quad (72)$$

which is exactly the Regge–Wheeler potential for a Schwarzschild background, as expected, since in this limit $f_{\text{GD}}(r)$ reverts to the Schwarzschild metric function $f_{\text{Schw}}(r)$. Looking at Fig. 4, it is possible to see this smooth transition as α bounces from the infimum to the supremum of the interval $[0.0, 1.0]$. The behavior of the GD and the seed potentials is essentially the same, but higher values of α yield lower maximum values in the GD potentials. In other words, the presence of α diminishes the potential barrier, which assumes its higher maximum value for $\alpha = 0$, i.e., in the Schwarzschild case.

The transition to the seed solution is not always monotonic. Take the potentials V_{GD_2} and V_{GD_3} in Figs. 5 and 6, respectively. The behavior for $\alpha > 0$ starts the same but deviates more and more as it approaches $r \rightarrow 3$ from $+\infty$. Starting at $\alpha = 0$, the next increment in α leads to the lowest

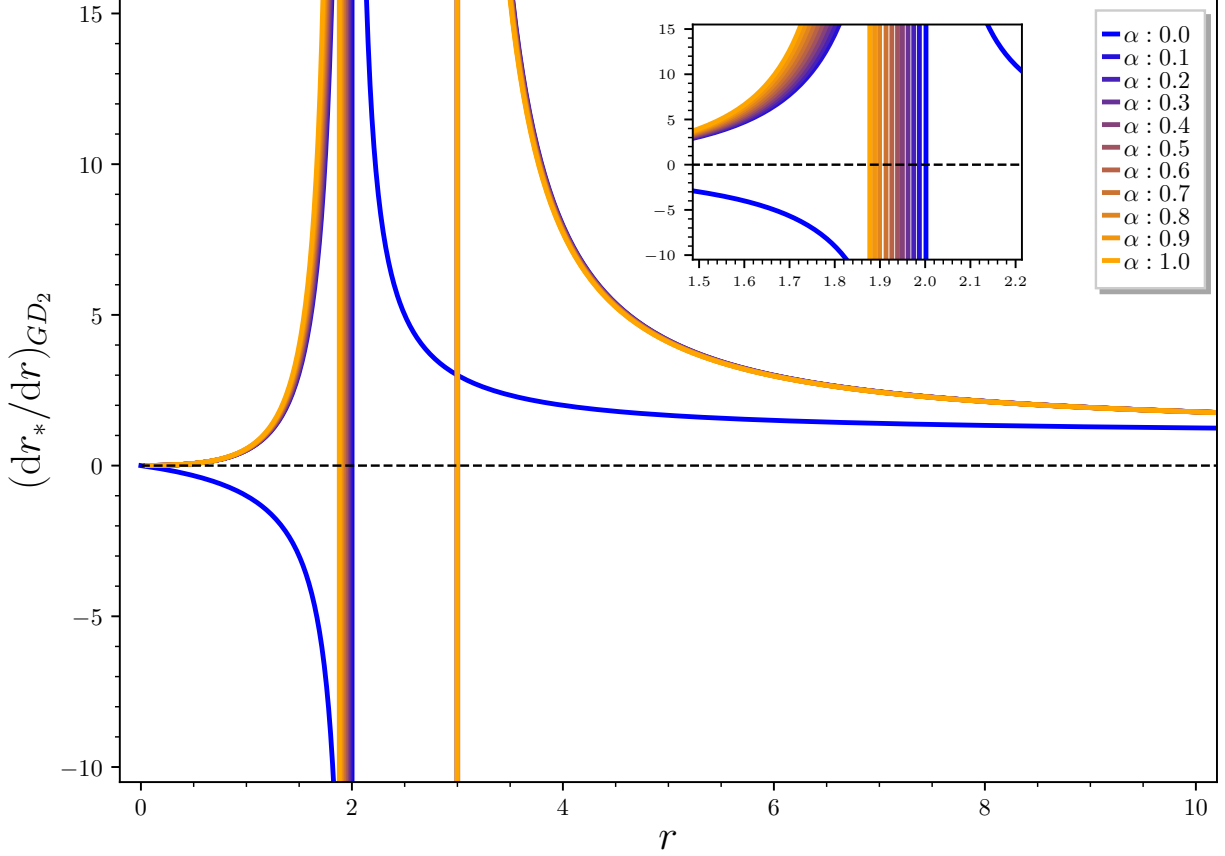


FIG. 2: Behaviour of $(dr_*/dr)_{GD_2} = f_{GD_2}^{-1}$ as a function of r for different values of α , in units of M , and $n = 2$. The event horizon is always at $r = 3$, except for $\alpha = 0$, but the Cauchy horizon assumes smaller values for larger α , where $\alpha = 0$ corresponds to the Schwarzschild spacetime.

maximum values of the GD potentials. Subsequent increments elevate the potential barriers, with a peak at $\alpha = 1.0$, in the $\alpha > 0$ regime. Thus, starting at $\alpha = 1.0$, the maximum values of V_{GD_2} and V_{GD_3} decrease as α decreases, but as soon as α reaches zero, they jump to the Schwarzschild case, where they assume their highest possible value. Hence, the maximum values of V_{GD_2} and V_{GD_3} , for all $\alpha > 0$ will be lower with respect to the Schwarzschild potential. However, between GD potentials, higher α values yield higher potential maximum values. Hence, even with different responses for $\alpha \in [0.1, 1.0]$, all three GD potentials agree with the fact that α effectively lowers the potential barrier.

V. QNMS OF GD HAIRY BLACK HOLES

In this section, the QNMs modes from the GD potentials will be computed and analyzed.

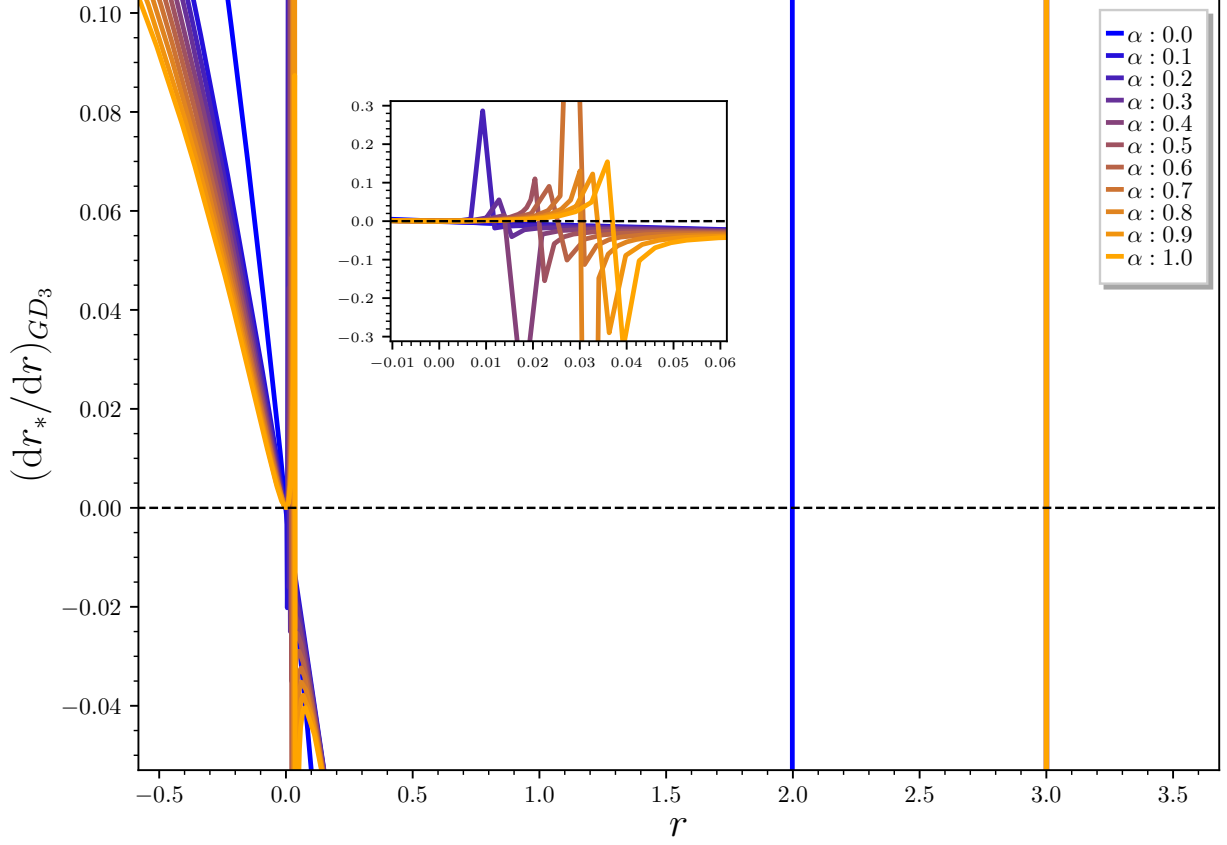


FIG. 3: Behaviour of $(dr_*/dr)_{GD_3} = f_{GD_3}^{-1}$ as a function of r for different values of α , in units of M , and $n = 2$. The event horizon is always at $r = 3$, except for $\alpha = 0$, but the Cauchy horizon assumes larger values for larger α , where $\alpha = 0$ corresponds to the Schwarzschild spacetime.

A. Hairy black hole QNM frequencies

Hereon we implement the sixth-order WKB approximation [53, 84] to derive the QNMs from the GD potentials. The complex frequencies in this method are given by

$$\omega^2 = V_0 - \frac{i}{2} \sqrt{V_0''} \left(\Lambda_2 + \Lambda_3 + \Lambda_4 + \Lambda_5 + \Lambda_6 + n_0 + \frac{1}{2} \right), \quad (73)$$

where V_0 represents the potential evaluated at its maximum, V_0'' represents its second derivative also evaluated at its maximum, and where Λ_i are the correction factors, which explicit forms can be found in Ref. [73].

Taking the necessary derivatives of V_{GD_1} and plugging them into the square root of Eq. (73) gives us the QNMs depicted in Fig. 7 and displayed in Tables V – VII for multiple values of harmonics n , overtone number n_0 and for $\alpha \in [0.1, 1.0]$ in a 0.1 partition grid, maintaining $n_0 \leq n$, where the method is suggested to be more accurate [10, 73, 85–87]. In this case, we have a fixed

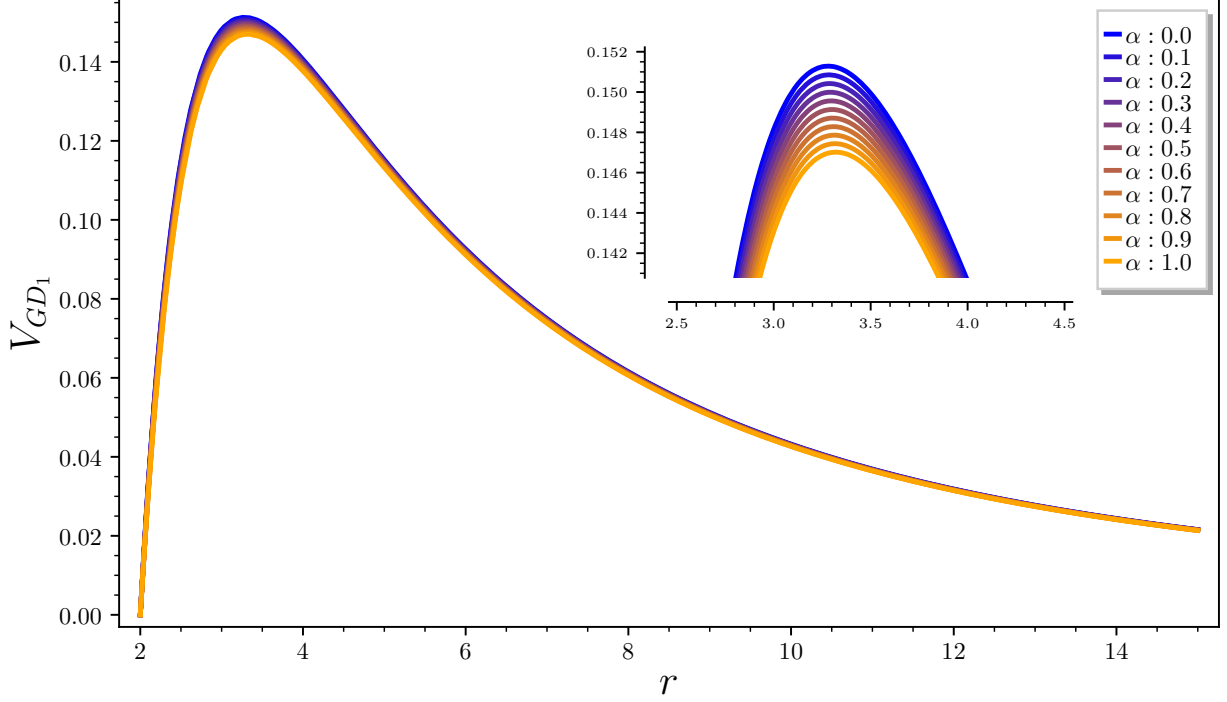


FIG. 4: Potential V_{GD_1} as a function of r , in units of M , for multiple values of α , with fixed $r_+ = 2$.

$\ell = e^{-2}$, and the first thing to notice is that for fixed values of α and harmonic n , the imaginary part of the modes increases with the overtone number n_0 , as expected from the definition of the overtones [73, 88], while the real part decreases. For fixed $\{\alpha, n_0\}$, the absolute values of both real and imaginary parts increase for higher harmonics. However, for fixed $\{n, n_0\}$, $|\text{Im}(\omega)|$ decreases with higher values α , as does its real part; ergo, the coupling constant α slows the decay of the overtones. Therefore, the solutions given by f_{GD_1} for each $\alpha > 0$ oscillate at a slower rate, but will oscillate longer than a Schwarzschild black hole. This result is similar to the ones obtained for scalar perturbations in Refs. [47, 53] with sixth and higher orders of the WKB method for the same hairy metric function f_{GD_1} .

The complex frequencies obtained for f_{GD_2} are displayed in Fig. 8 and Tables VIII – X, for the same range of values of $\{\alpha, n, n_0\}$ used for f_{GD_1} , and fixed event horizon $r_+ = \alpha\ell = 3$, in units of M . In this set, we encounter the same results for fixed α , but in contrast with V_{GD_1} , the damping grows with the increase of α . Therefore, GD solutions by f_{GD_2} for $\alpha > 0$ seem to oscillate and fade more rapidly with higher values of the α parameter.

As for f_{GD_3} , the behaviour of its QNMs, seen in Fig. 9 and Tables XI – XIII, is very similar to those of f_{GD_2} , with some distinctive traits. For fixed $\{\alpha, n\}$, the real part decreases, while the

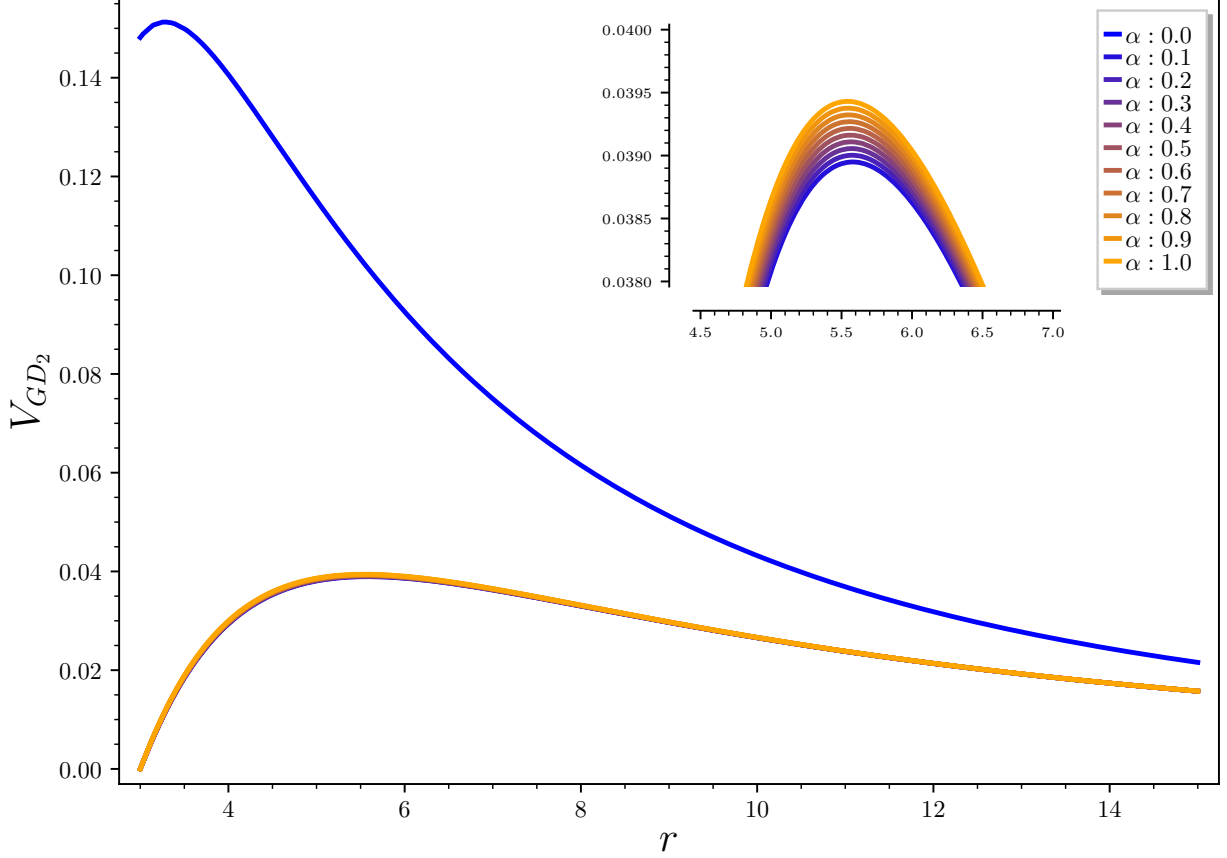


FIG. 5: Potential V_{GD_2} as a function of r , in units of M , for multiple values of α , with fixed $r_+ = \alpha\ell = 3$.

imaginary part increases for higher n_0 , once again, as expected. For fixed $\{n, n_0\}$, as obtained for f_{GD_2} , the imaginary part increases in absolute value as α increases. The real part of the frequencies increases in the overall range $\alpha \in [0.1, 1.0]$ for lower overtones, but decreases for higher overtones, which is the region where the method has lower accuracy. Thus, this anomaly may be related to shortcomings of the method or even due to the order implemented.

For both V_{GD_2} and V_{GD_3} , a drop in range for both parts of the complex frequencies with respect to the Schwarzschild case is observed. This gap is slightly smaller for V_{GD_3} , compared with the one observed for V_{GD_2} , which may be caused by the different forms of the GD potentials, or due to the different values of $\alpha\ell$ used. Since we chose to perform our analysis in a regime of a fixed event horizon, in order to keep $r_+ = 3$, $\alpha\ell$ must equal 3 for f_{GD_2} and equal 1 for f_{GD_3} . Given what has been observed so far from α , it is reasonable to expect the gap between the deformed potentials and the Schwarzschild case to increase as α increases, for fixed ℓ .

Our initial analysis of the GD potentials showed a clear distinction between their maximum

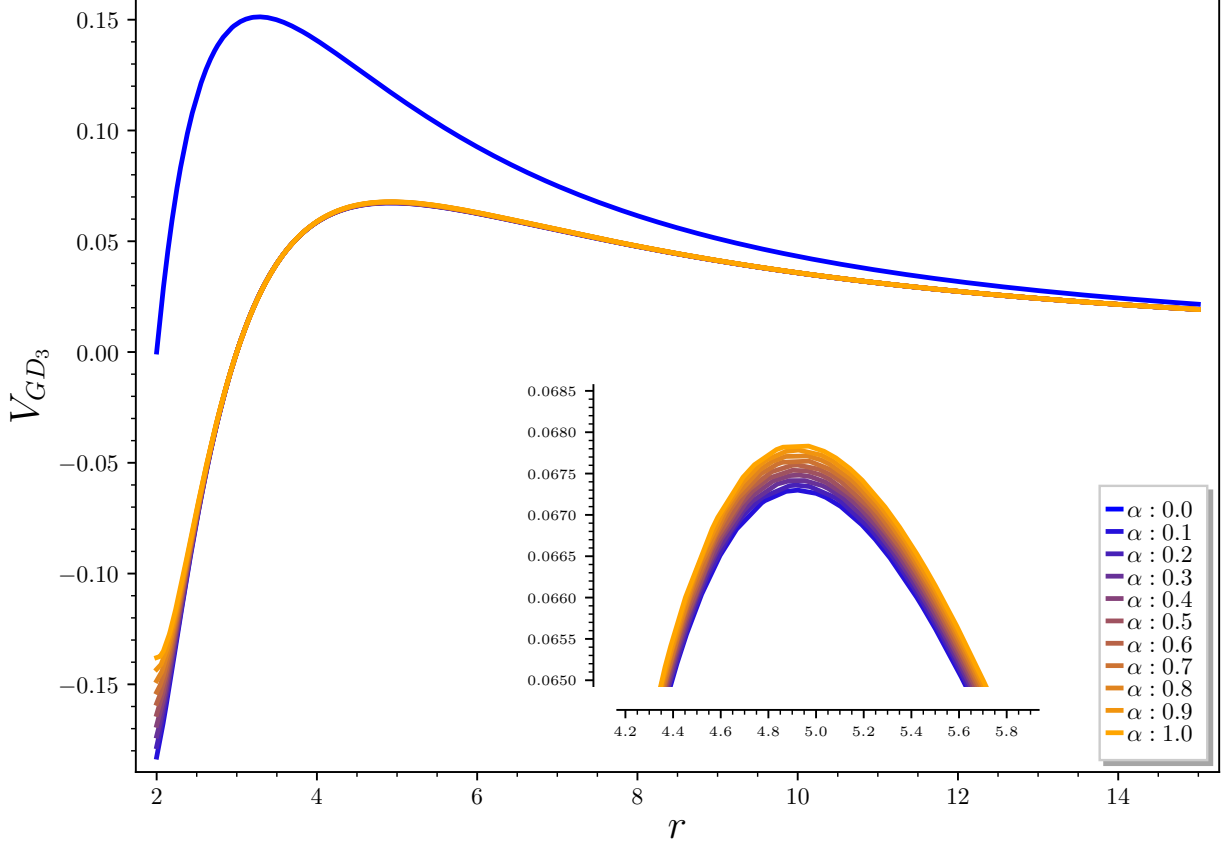


FIG. 6: Potential V_{GD_3} as a function of r , in units of M , for multiple values of α , with fixed $r_+ = 2 + \alpha\ell = 3$.

values, in comparison with the Schwarzschild odd potential. Despite the transition from the hairy to the no-hair values being monotonic for V_{GD_1} , but not for $\{V_{GD_2}, V_{GD_3}\}$, all three GD potentials presented lower maximum values, for all values of α different than zero. This feature seems to be carried through the calculations of the WKB method, and reflected in the complex frequencies especially in their imaginary parts. Therefore, our analysis has led us to conclude that, despite their particularities inside the $\alpha > 0$ regime, GD hairy black holes satisfying the DEC have lower damping rates than a Schwarzschild black hole.

B. The Spectrum of no-hair black holes with the same $\{r_+, Q^2\}$

A natural question to ponder is whether the spectrum just obtained is exclusive to the GD hairy black hole solutions presented. In other words, is it possible for a no-hair solution to reproduce the same spectrum with some combination of its parameters? To start addressing this issue, we call back to Eq. (59), from which we conclude that both RN and GD spacetimes cannot have the

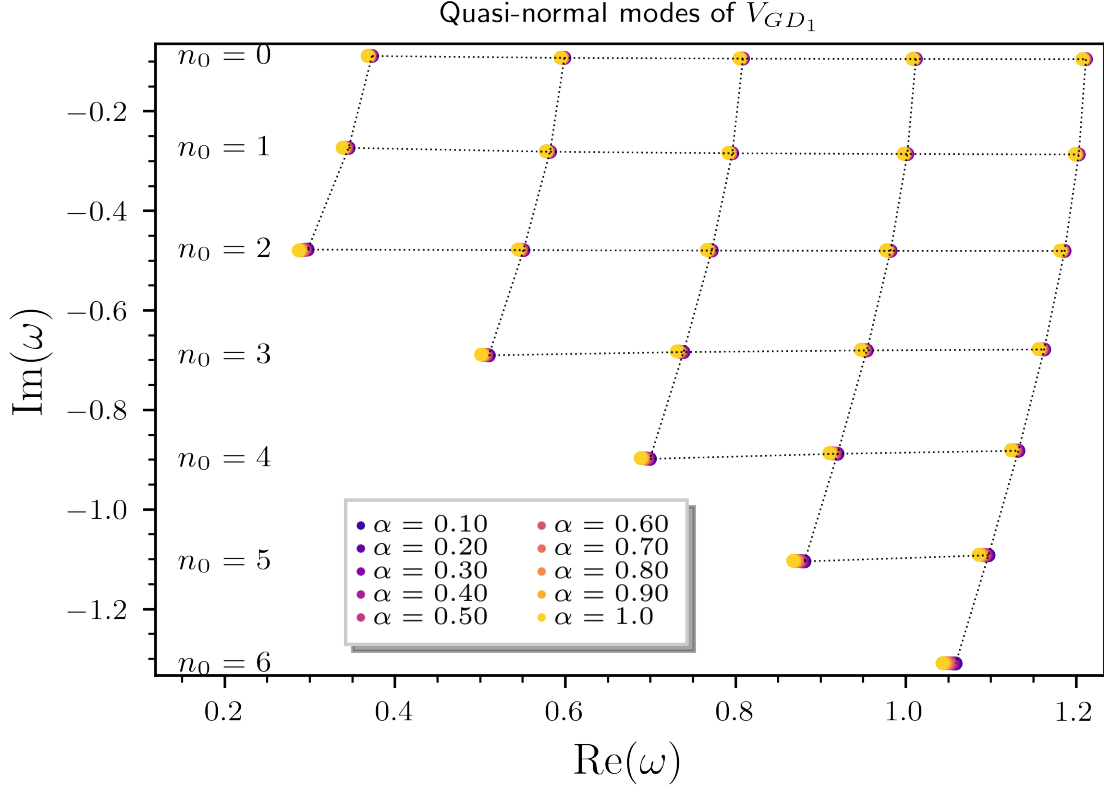


FIG. 7: QNMs of the potential V_{GD_1} for a range of values of α . The vertical dotted lines correspond, from left to right, to the harmonic number $n = 2, 3, 4, 5$ and 6 respectively. The horizontal lines correspond to the displayed overtone.

same values for all three parameters $\{r_+, M, Q^2\}$ while having $\alpha \neq 0$. So, one must choose a combination of two out of the three parameters. In this paper we will work with RN black holes with equivalent values for the square of its charge Q^2 , and outer horizon $r_+ = \{2, 3\}$, from the GD potentials. The goal is to obtain the QNMs for the RN black holes with same $\{r_+, Q^2\}$ and compare them with those obtained from the corresponding GD black holes.

For the metric function f_{RN} , the outer horizon is given by:

$$r_+ = \bar{M} + \sqrt{\bar{M}^2 - \bar{Q}^2}, \quad (74)$$

where $\{\bar{M}, \bar{Q}\}$ are the mass and electric charge of the no-hair RN spacetime. Solving for \bar{M} , we get:

$$2\bar{M} = \frac{\bar{Q}^2}{r_+} + r_+. \quad (75)$$

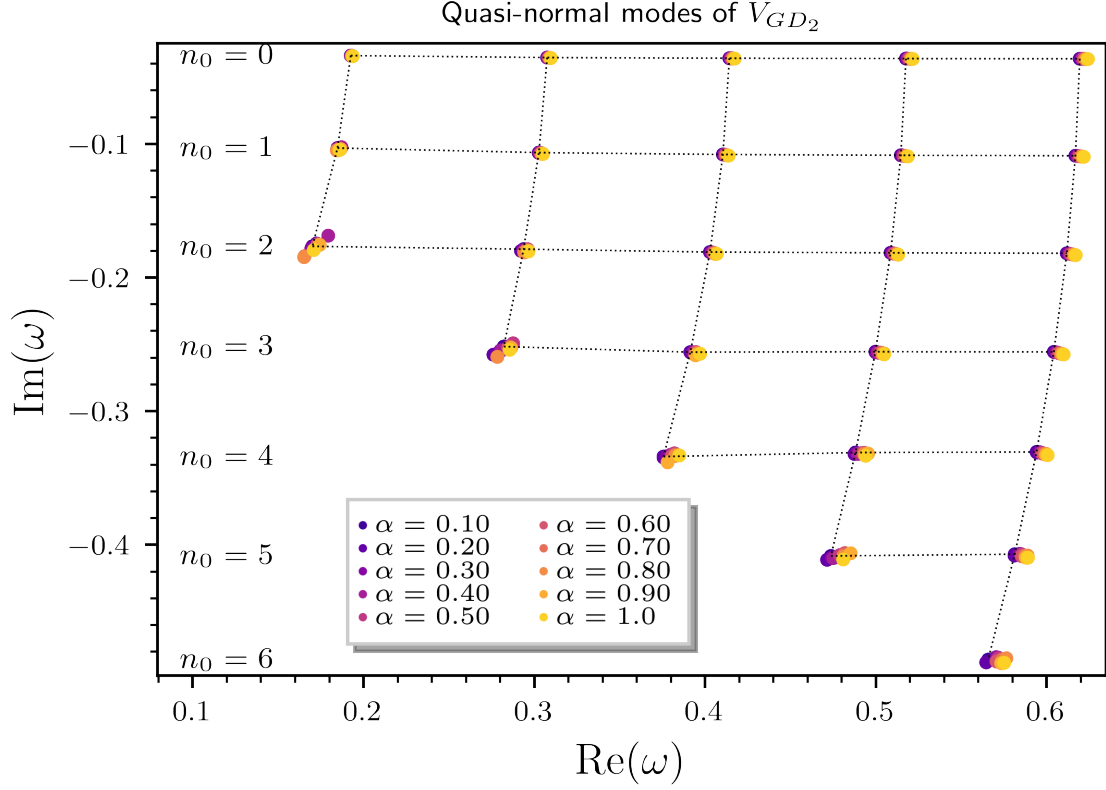


FIG. 8: QNMs of the potential V_{GD_2} for a range of values of α . The vertical dotted lines correspond, from left to right, to the harmonic numbers $n = 2, 3, 4, 5$ and 6 respectively. The horizontal lines correspond to the displayed overtone.

For $\bar{Q}^2 = Q^2$, from Eqs. (52a), (52b), and (52c), we obtain:

$$\bar{M}_1 = \alpha e^{-2} + 1, \quad (76)$$

$$\bar{M}_2 = \frac{1}{2} (5 + \alpha e^{-3}), \quad (77)$$

$$\bar{M}_3 = \frac{1}{2} (3 + \alpha e^{-3}), \quad (78)$$

where we substituted $r_+ = 2$ for \bar{M}_1 , and $r_+ = 3$ for \bar{M}_2 and \bar{M}_3 .

Substituting Eqs. (76) – (78) back into f_{GD_1} , f_{GD_2} , and f_{GD_3} , respectively, and plugging the new metric functions into Eq. (70), gives us the odd potentials V_{RN_1} , V_{RN_2} and V_{RN_3} . These are odd-RN potentials, with same values for r_+ and charge Q^2 as V_{GD_1} , V_{GD_2} and V_{GD_3} , respectively. Their QNMs are obtained by taking the necessary derivatives and substituting them into Eq. (73), which will then yield their complex frequencies. Our goal is to see how close these frequencies are

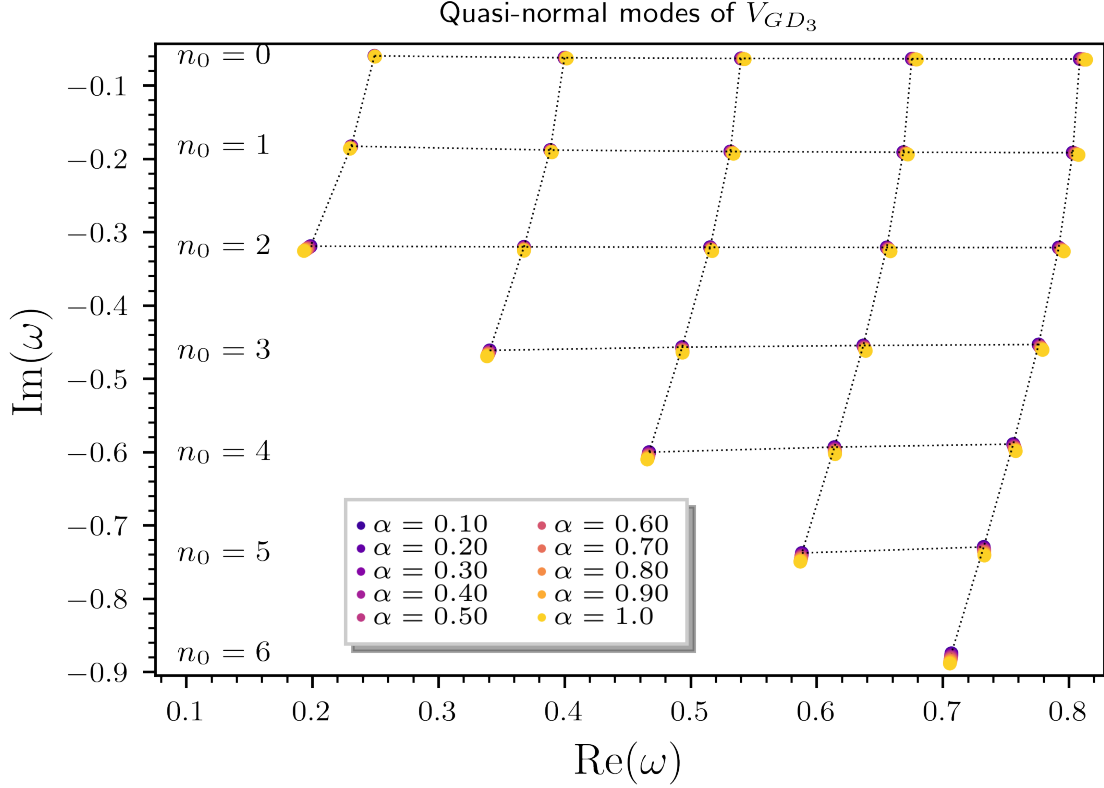


FIG. 9: QNMs of the potential V_{GD_3} for a range of values of α . The vertical dotted lines correspond, from left to right, to the harmonic number $n = 2, 3, 4, 5$ and 6 respectively. The horizontal lines correspond to the displayed overtone.

to the ones we obtained for the GD potentials. To this end, we define:

$$\Delta\omega \equiv |\omega_{GD} - \omega_{RN}|, \quad (79)$$

which we obtain for each pair $\{V_{GD_i}, V_{RN_i}\}$, for $i = \{1, 2, 3\}$, i.e., a GD potential and a correspondent RN potential with the same values for r_+ and Q^2 . The results depicted in Figs. 10 – 12 and which compose the tables of Appendix C tell us that, for all three pairs $\{V_{GD_i}, V_{RN_i}\}$, the absolute value $|\Delta\text{Im}(\omega)|$ increases as α increases, i.e., the imaginary parts are more distinguished from each other for higher values of the primary hair α , for a given pair $\{n, n_0\}$.

In Tables I and II we present the difference of the imaginary parts of the fundamental modes, for $\alpha \in [0.1, 0.5]$ and $\alpha \in [0.6, 1.0]$, respectively, in a 0.1 partition grid.

The values from the two potentials deviate approximately ten times more for $\alpha = 1.0$, in comparison with $\alpha = 0.1$, which hints at the influence of the primary hair in distinguishing the GD potential from the RN potential. However, to ratify these results, we need to know the magnitude

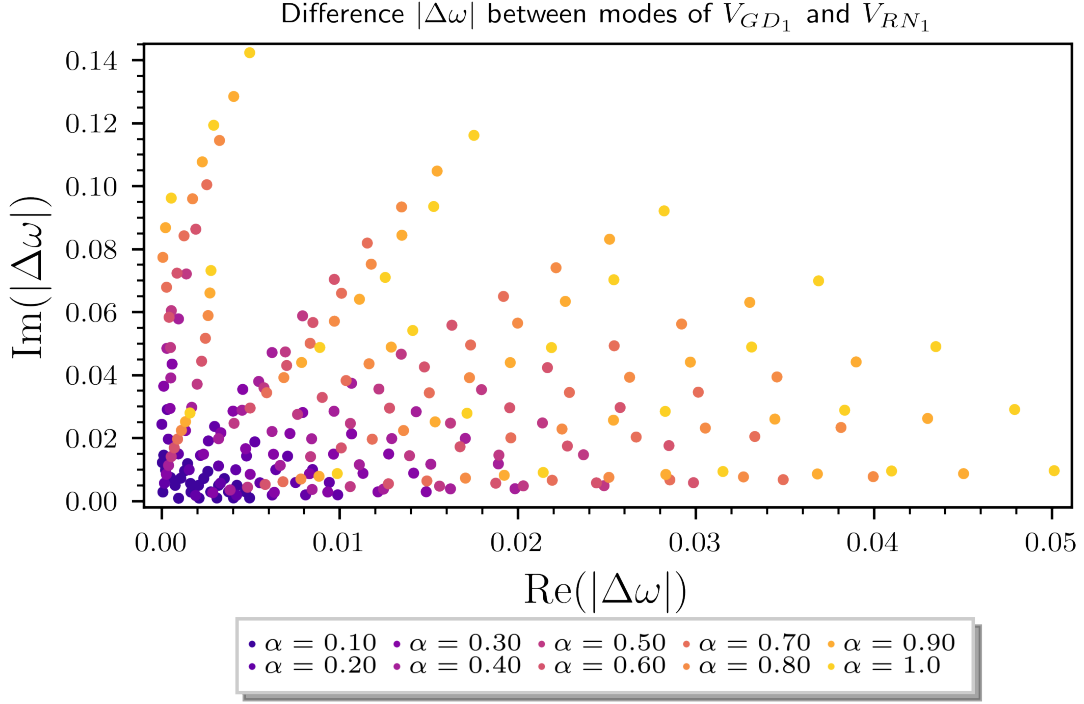


FIG. 10: QNMs difference ($\Delta\omega$) for the potentials V_{GD_1} and V_{RN_1} for a range of values of α . It corresponds to the data shown in Tables XIV, XV, XVI and XVII.

TABLE I: Absolute values of $\Delta\text{Im}(\omega)$ for the pair $\{V_{GD_1}, V_{RN_1}\}$, $n_0 = 0$ and $\alpha \in \{0.1, 0.2, 0.3, 0.4, 0.5\}$.

n	$\alpha = 0.1$	$\alpha = 0.2$	$\alpha = 0.3$	$\alpha = 0.4$	$\alpha = 0.5$
2	8.83×10^{-4}	1.76×10^{-3}	2.64×10^{-3}	3.52×10^{-3}	4.39×10^{-3}
3	9.22×10^{-4}	1.84×10^{-3}	2.76×10^{-3}	3.67×10^{-3}	4.58×10^{-3}
4	9.53×10^{-4}	1.90×10^{-3}	2.85×10^{-3}	3.79×10^{-3}	4.73×10^{-3}
5	9.71×10^{-4}	1.94×10^{-3}	2.90×10^{-3}	3.86×10^{-3}	4.82×10^{-3}
6	9.81×10^{-4}	1.96×10^{-3}	2.93×10^{-3}	3.90×10^{-3}	4.87×10^{-3}

of the error of the WKB method at the sixth-order for this potential. This can be achieved by implementing the WKB method to one order higher and one order lower, such that:

$$\delta_k = \frac{1}{2}(\omega_{k+1} - \omega_{k-1}), \quad (80)$$

where k is the order of the WKB method, δ_k is the error correspondent to that order, and ω_{k+1} and ω_{k-1} are the complex frequencies obtained by the WKB method in the $k+1$ and $k-1$ orders, respectively, as proposed and shown to be a good estimation in [84]. Setting $k = 6$, Eq. (80)

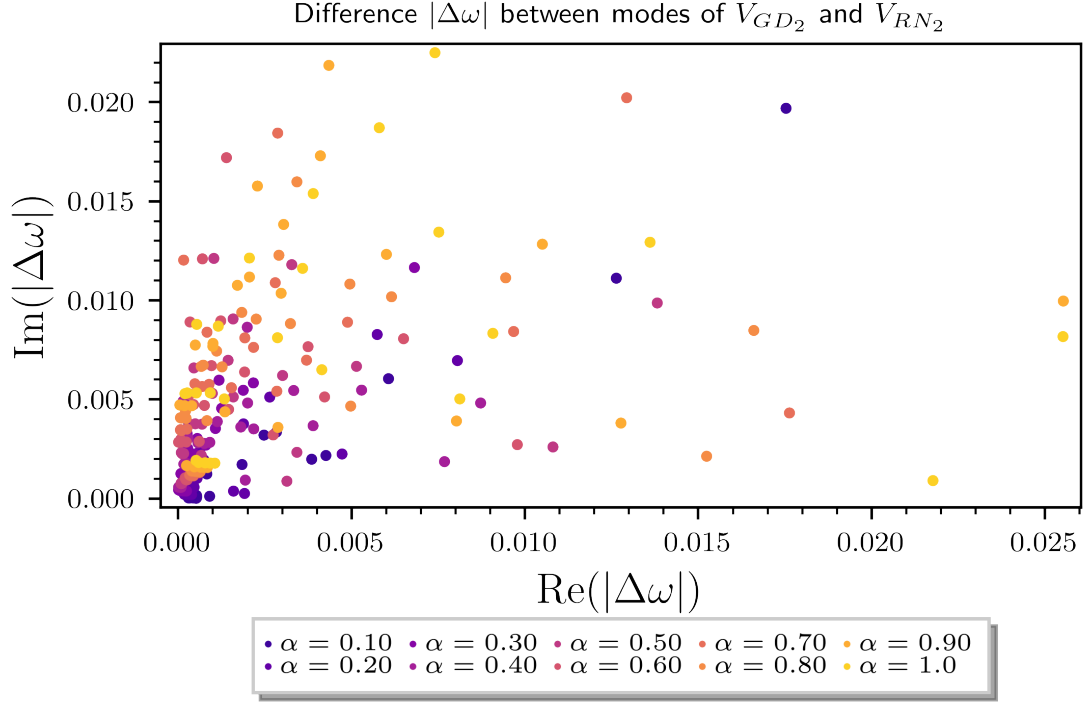


FIG. 11: QNMs difference ($\Delta\omega$) for the potentials V_{GD_2} and V_{RN_2} for a range of values of α . It corresponds to the data shown in Tables XVIII, XIX, XX and XXI.

TABLE II: Absolute values of $\Delta\text{Im}(\omega)$ for the pair $\{V_{GD_1}, V_{RN_1}\}$, $n_0 = 0$ and $\alpha \in \{0.6, 0.7, 0.8, 0.9, 1.0\}$.

n	$\alpha = 0.6$	$\alpha = 0.7$	$\alpha = 0.8$	$\alpha = 0.9$	$\alpha = 1.0$
2	5.26×10^{-3}	6.13×10^{-3}	6.99×10^{-3}	7.85×10^{-3}	8.71×10^{-3}
3	5.48×10^{-3}	6.39×10^{-3}	7.28×10^{-3}	8.18×10^{-3}	9.07×10^{-3}
4	5.67×10^{-3}	6.60×10^{-3}	7.52×10^{-3}	8.44×10^{-3}	9.36×10^{-3}
5	5.77×10^{-3}	6.72×10^{-3}	7.66×10^{-3}	8.60×10^{-3}	9.53×10^{-3}
6	5.83×10^{-3}	6.79×10^{-3}	7.74×10^{-3}	8.69×10^{-3}	9.63×10^{-3}

becomes:

$$\delta_6 = \frac{1}{2} (\omega_7 - \omega_5). \quad (81)$$

In Tables III and IV, we present the error obtained from Eq. (81) for the imaginary parts of the fundamental modes of the GD potential V_{GD_1} at sixth-order in the WKB method. Comparing Tables I and II with Tables III and IV, we see that $\Delta\omega$ is two to four orders of magnitude higher than δ_6 , which shows that a comparative spectroscopic analysis of QNMs is indeed capable of distinguishing the GD hairy black hole solutions here presented from possible no-hair solutions, at

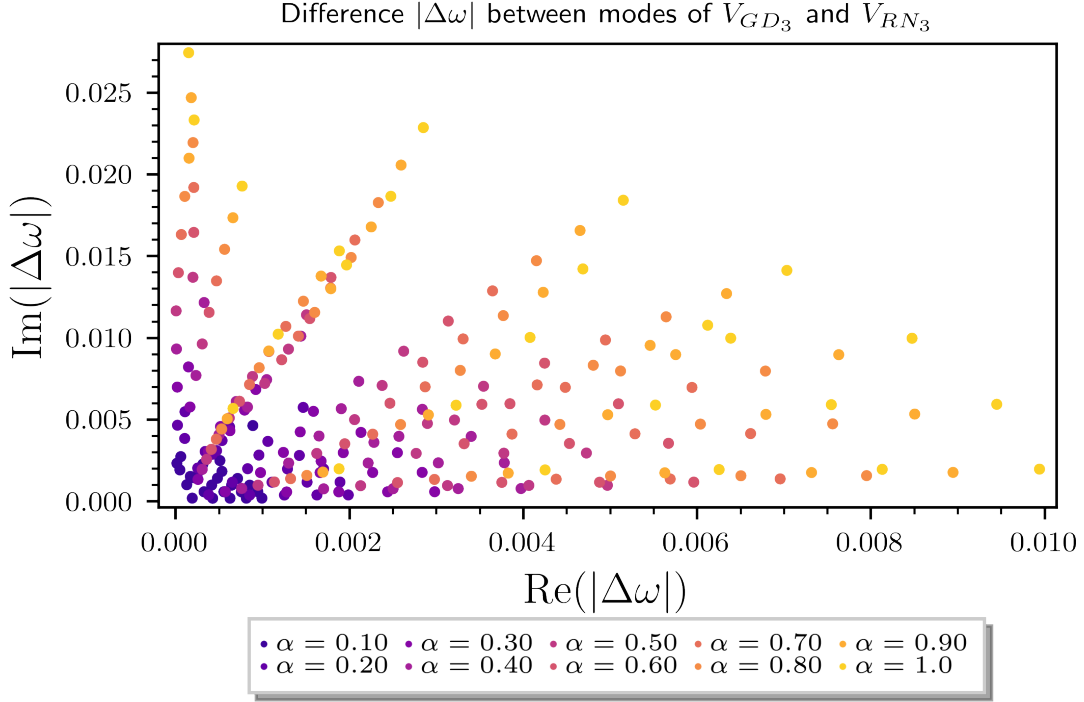


FIG. 12: QNMs difference ($\Delta\omega$) for the potentials V_{GD_3} and V_{RN_3} for a range of values of α . It corresponds to the data shown in Tables [XXII](#), [XXIII](#), [XXIV](#) and [XXV](#).

TABLE III: Imaginary parts of δ_6 for V_{GD_1} , $n_0 = 0$, and $\alpha \in \{0.1, 0.2, 0.3, 0.4, 0.5\}$.

n	$\alpha = 0.1$	$\alpha = 0.2$	$\alpha = 0.3$	$\alpha = 0.4$	$\alpha = 0.5$
2	6.05×10^{-5}	6.34×10^{-5}	6.67×10^{-5}	7.23×10^{-5}	7.57×10^{-5}
3	4.37×10^{-8}	7.15×10^{-8}	1.96×10^{-7}	2.20×10^{-7}	9.84×10^{-8}
4	6.48×10^{-8}	9.91×10^{-8}	1.00×10^{-7}	1.45×10^{-7}	1.28×10^{-7}
5	2.66×10^{-8}	2.61×10^{-8}	2.82×10^{-8}	3.17×10^{-8}	3.78×10^{-8}
6	9.90×10^{-9}	1.18×10^{-8}	1.14×10^{-8}	1.15×10^{-8}	1.63×10^{-8}

least in the context where such solutions possess the same values for $\{r_+, Q^2\}$.

VI. CONCLUSIONS

The results presented here attest to the promising nature of the GD method in decoupling sources of gravity and, in the process, producing charges capable of generating primary hair, and the relevance of studying the QNMs of these hairy solutions. We conclude that the hairy solutions generated by the GD method can be considered different enough from no-hair black holes with the

TABLE IV: Imaginary parts of δ_6 for V_{GD_1} , $n_0 = 0$, and $\alpha \in \{0.6, 0.7, 0.8, 0.9, 1.0\}$.

n	$\alpha = 0.6$	$\alpha = 0.7$	$\alpha = 0.8$	$\alpha = 0.9$	$\alpha = 1.0$
2	8.07×10^{-5}	8.47×10^{-5}	8.98×10^{-5}	9.54×10^{-5}	9.97×10^{-5}
3	3.92×10^{-7}	2.39×10^{-7}	4.16×10^{-7}	1.80×10^{-7}	3.62×10^{-7}
4	1.64×10^{-7}	1.62×10^{-7}	1.83×10^{-7}	2.05×10^{-7}	1.13×10^{-7}
5	4.70×10^{-8}	4.29×10^{-8}	6.43×10^{-8}	4.10×10^{-8}	3.84×10^{-8}
6	1.78×10^{-8}	1.03×10^{-8}	1.96×10^{-8}	1.71×10^{-8}	2.57×10^{-8}

same $\{r_+, Q^2\}$ to be recognized by the spectra of their QNMs alone, since the difference between the solutions could not be attributed to the method inaccuracy. Thus, confirming $\Delta\omega$ as a hair signature in an observable quantity, e.g., the black hole QNMs.

Acknowledgements

VFG thanks CAPES (Grant No. 001). RTC thanks the National Council for Scientific and Technological Development - CNPq (Grant No. 401567/2023-0), for partial financial support. RC thanks the National Council for Scientific and Technological Development – CNPq (Grant No. 401567/2023-0). The work of RdR is supported by The São Paulo Research Foundation (FAPESP) (Grants No. 2021/01089-1 and No. 2024/05676-7) and CNPq (Grants No. 303742/2023-2 and No. 401567/2023-0).

Appendix A: The Odd GD Potentials

Here we present the GD potentials V_{GD_1} , V_{GD_2} and V_{GD_3} in their explicit forms, obtained by substituting the GD metric functions f_{GD_1} , f_{GD_2} and f_{GD_3} into Eq. (70), respectively.

$$\begin{aligned}
 V_{\text{GD}_1}(r) = & \left\{ \left(1 - \frac{2}{r}\right) \left(\frac{n(n+1)}{r^2} - \frac{6}{r^3}\right) \right\} - \\
 & - \alpha \left\{ \left[\frac{1}{2r} + \frac{n(n+1)-1}{r^3} + \frac{1}{r^2} - \frac{12}{r^4} \right] e^{(-r)} + \right. \\
 & + \left. \left[n(n+1) \left(\frac{1}{r^3} - \frac{4}{r^4} \right) + \frac{3}{r^3} - \frac{28}{r^4} + \frac{56}{r^5} \right] e^{(-2)} \right\} + \\
 & + \alpha^2 \left\{ \left(\frac{3}{r^4} - \frac{28}{r^5} + \frac{64}{r^6} \right) e^{(-4)} + \frac{1}{2} \left(\frac{1}{r^2} + \frac{4}{r^3} + \frac{6}{r^4} \right) e^{(-2r)} + \right. \\
 & + \left. \frac{1}{2} \left(\frac{1}{r^2} - \frac{4}{r^4} - \frac{56}{r^5} \right) e^{(-r-2)} \right\}, \tag{A1}
 \end{aligned}$$

$$\begin{aligned}
 V_{\text{GD}_2}(r) = & \left\{ \left(1 - \frac{2}{r}\right) \left(\frac{n(n+1)}{r^2} - \frac{6}{r^3}\right) \right\} - \\
 & - \alpha \left\{ \left[\frac{1}{2r} + \frac{n(n+1)-1}{r^3} + \frac{1}{r^2} - \frac{12}{r^4} \right] e^{(-r)} + \right. \\
 & + \left. \ell \left[n(n+1) \left(\frac{1}{r^3} - \frac{2}{r^4} \right) + \frac{3}{r^3} - \frac{20}{r^4} + \frac{28}{r^5} \right] \right\} + \\
 & + \alpha^2 \left\{ \ell \left[\left(\frac{n(n+1)}{r^4} + \frac{4}{r^4} - \frac{14}{r^5} \right) e^{(-\alpha\ell)} + \frac{1}{2} \left(\frac{1}{r^2} + \frac{2}{r^3} + \frac{4}{r^4} - \frac{28}{r^5} \right) e^{(-r)} \right] + \right. \\
 & + \left. \ell^2 \left(\frac{3}{r^4} - \frac{14}{r^5} + \frac{16}{r^6} \right) + \frac{1}{2} \left(\frac{1}{r^2} + \frac{4}{r^3} + \frac{6}{r^4} \right) e^{(-2r)} \right\} - \\
 & - \alpha^3 \left\{ \ell^2 \left(\frac{7}{r^5} - \frac{16}{r^6} \right) e^{(-\alpha\ell)} + \ell \left(\frac{1}{2r^3} + \frac{4}{r^4} + \frac{14}{r^5} \right) e^{(-\alpha\ell-r)} \right\} + \\
 & + \alpha^4 \left(\frac{4\ell^2 e^{(-2\alpha\ell)}}{r^6} \right), \tag{A2}
 \end{aligned}$$

$$\begin{aligned}
V_{\text{GD}_3}(r) = & \left\{ \left(1 - \frac{2}{r} \right) \left(\frac{n(n+1)}{r^2} - \frac{6}{r^3} \right) \right\} - \\
& - \alpha \left\{ \left[\frac{1}{2r} + \frac{n(n+1)-1}{r^3} + \frac{1}{r^2} - \frac{12}{r^4} \right] e^{(-r)} + \right. \\
& + \ell \left(\frac{n(n+1)}{r^3} + \frac{3}{r^3} - \frac{12}{r^4} \right) - 2 \left(\frac{n(n+1)}{r^4} + \frac{4}{r^4} - \frac{14}{r^5} \right) e^{(-\alpha\ell-2)} \Big\} + \\
& + \alpha^2 \left\{ \ell \left[\left(\frac{n(n+1)}{r^4} + \frac{4}{r^4} - \frac{28}{r^5} \right) e^{(-\alpha\ell-2)} + \left(\frac{1}{2r^2} + \frac{2}{r^3} + \frac{6}{r^4} \right) e^{(-r)} \right] + \right. \\
& + \left(\frac{1}{2r^2} + \frac{2}{r^3} + \frac{3}{r^4} \right) e^{(-2r)} - \left(\frac{1}{r^3} + \frac{4}{r^4} + \frac{14}{r^5} \right) e^{(-\alpha\ell-r-2)} + \\
& + \frac{16e^{(-2\alpha\ell-4)}}{r^6} + \frac{3\ell^2}{r^4} \Big\} - \\
& - \alpha^3 \left\{ \ell \left[\left(\frac{1}{2r^3} + \frac{2}{r^4} + \frac{7}{r^5} \right) e^{(-\alpha\ell-r-2)} - \frac{16e^{(-2\alpha\ell-4)}}{r^6} \right] + \frac{7\ell^2 e^{(-\alpha\ell-2)}}{r^5} \right\} + \\
& + \alpha^4 \left(\frac{4\ell^2 e^{(-2\alpha\ell-4)}}{r^6} \right).
\end{aligned} \tag{A3}$$

Appendix B: QNMs from GD Potentials

We now display the real and imaginary parts of the complex frequencies that compose the QNMs obtained through the sixth-order WKB method applied to the GD potentials V_{GD_1} , V_{GD_2} and V_{GD_3} , whose explicit forms can be found in Appendix A.

QNMs from V_{GD_1}

n	n_0	$\alpha = 0.0$		$\alpha = 0.1$		$\alpha = 0.2$		$\alpha = 0.3$	
		$\text{Re}(\omega)$	$\text{Im}(\omega)$	$\text{Re}(\omega)$	$\text{Im}(\omega)$	$\text{Re}(\omega)$	$\text{Im}(\omega)$	$\text{Re}(\omega)$	$\text{Im}(\omega)$
2	0	0.37362	-0.08889	0.37303	-0.08886	0.37243	-0.08883	0.37184	-0.08880
	1	0.34630	-0.27348	0.34553	-0.27343	0.34475	-0.27338	0.34398	-0.27334
	2	0.29852	-0.47756	0.29739	-0.47774	0.29625	-0.47792	0.29509	-0.47811
3	0	0.59944	-0.09270	0.59894	-0.09267	0.59844	-0.09264	0.59794	-0.09260
	1	0.58264	-0.28129	0.58208	-0.28119	0.58151	-0.28109	0.58094	-0.28099
	2	0.55159	-0.47905	0.55088	-0.47888	0.55016	-0.47872	0.54945	-0.47856
	3	0.51110	-0.69047	0.51012	-0.69028	0.50914	-0.69009	0.50816	-0.68990
4	0	0.80918	-0.09416	0.80871	-0.09414	0.80824	-0.09412	0.80777	-0.09409
	1	0.79663	-0.28433	0.79611	-0.28426	0.79558	-0.28419	0.79506	-0.28411
	2	0.77270	-0.47990	0.77205	-0.47977	0.77140	-0.47964	0.77076	-0.47951
	3	0.73966	-0.68390	0.73881	-0.68372	0.73794	-0.68354	0.73708	-0.68337
	4	0.70064	-0.89846	0.69944	-0.89827	0.69823	-0.89807	0.69702	-0.89789
5	0	1.01230	-0.09487	1.01183	-0.09485	1.01136	-0.09484	1.01090	-0.09482
	1	1.00222	-0.28582	1.00171	-0.28576	1.00119	-0.28571	1.00068	-0.28565
	2	0.98269	-0.48033	0.98208	-0.48023	0.98146	-0.48013	0.98085	-0.48004
	3	0.95496	-0.68054	0.95417	-0.68040	0.95338	-0.68026	0.95259	-0.68013
	4	0.92081	-0.88819	0.91975	-0.88802	0.91870	-0.88785	0.91764	-0.88769
	5	0.88238	-1.10445	0.88093	-1.10429	0.87947	-1.10414	0.87801	-1.10399
6	0	1.21201	-0.09527	1.21153	-0.09525	1.21105	-0.09524	1.21058	-0.09523
	1	1.20357	-0.28665	1.20306	-0.28661	1.20254	-0.28657	1.20202	-0.28653
	2	1.18707	-0.48056	1.18647	-0.48049	1.18586	-0.48042	1.18526	-0.48034
	3	1.16326	-0.67858	1.16251	-0.67847	1.16176	-0.67837	1.16101	-0.67826
	4	1.13323	-0.88208	1.13226	-0.88194	1.13130	-0.88180	1.13033	-0.88167
	5	1.09837	-1.09213	1.09710	-1.09197	1.09582	-1.09182	1.09454	-1.09168
	6	1.06023	-1.30946	1.05853	-1.30933	1.05683	-1.30922	1.05512	-1.30912

TABLE V: Real and imaginary parts from the QNMs of potential V_{GD_1} for $\alpha \in \{0.0, 0.1, 0.2, 0.3\}$ and $\ell = e^{-2}$.

QNMs from V_{GD_1}

n	n_0	$\alpha = 0.4$		$\alpha = 0.5$		$\alpha = 0.6$		$\alpha = 0.7$	
		$\text{Re}(\omega)$	$\text{Im}(\omega)$	$\text{Re}(\omega)$	$\text{Im}(\omega)$	$\text{Re}(\omega)$	$\text{Im}(\omega)$	$\text{Re}(\omega)$	$\text{Im}(\omega)$
2	0	0.37125	-0.08877	0.37065	-0.08875	0.37006	-0.08872	0.36946	-0.08870
	1	0.34320	-0.27330	0.34241	-0.27326	0.34162	-0.27323	0.34083	-0.27321
	2	0.29393	-0.47830	0.29276	-0.47850	0.29158	-0.47870	0.29038	-0.47891
3	0	0.59744	-0.09257	0.59694	-0.09253	0.59644	-0.09250	0.59594	-0.09247
	1	0.58038	-0.28088	0.57981	-0.28078	0.57924	-0.28068	0.57868	-0.28058
	2	0.54873	-0.47839	0.54801	-0.47823	0.54729	-0.47807	0.54656	-0.47791
	3	0.50717	-0.68971	0.50617	-0.68953	0.50518	-0.68934	0.50417	-0.68916
4	0	0.80730	-0.09407	0.80683	-0.09405	0.80636	-0.09402	0.80589	-0.09399
	1	0.79453	-0.28404	0.79401	-0.28396	0.79348	-0.28389	0.79296	-0.28382
	2	0.77011	-0.47939	0.76946	-0.47926	0.76881	-0.47913	0.76816	-0.47901
	3	0.73621	-0.68319	0.73534	-0.68302	0.73448	-0.68285	0.73360	-0.68268
	4	0.69580	-0.89771	0.69458	-0.89753	0.69335	-0.89736	0.69213	-0.89719
5	0	1.01043	-0.09480	1.00996	-0.09478	1.00950	-0.09477	1.00903	-0.09475
	1	1.00017	-0.28560	0.99965	-0.28555	0.99914	-0.28550	0.99863	-0.28544
	2	0.98023	-0.47995	0.97962	-0.47985	0.97900	-0.47976	0.97838	-0.47967
	3	0.95180	-0.67999	0.95101	-0.67986	0.95022	-0.67973	0.94942	-0.67960
	4	0.91657	-0.88753	0.91551	-0.88737	0.91444	-0.88722	0.91337	-0.88707
	5	0.87655	-1.10385	0.87508	-1.10372	0.87361	-1.10360	0.87213	-1.10349
6	0	1.21010	-0.09521	1.20962	-0.09520	1.20914	-0.09519	1.20867	-0.09517
	1	1.20150	-0.28649	1.20098	-0.28645	1.20046	-0.28641	1.19994	-0.28637
	2	1.18465	-0.48027	1.18405	-0.48020	1.18344	-0.48013	1.18283	-0.48006
	3	1.16026	-0.67816	1.15951	-0.67805	1.15876	-0.67795	1.15801	-0.67785
	4	1.12936	-0.88153	1.12839	-0.88141	1.12742	-0.88128	1.12645	-0.88116
	5	1.09326	-1.09154	1.09198	-1.09141	1.09069	-1.09129	1.08940	-1.09117
	6	1.05341	-1.30902	1.05169	-1.30894	1.04996	-1.30887	1.04823	-1.30881

TABLE VI: Real and imaginary parts from the QNMs of potential V_{GD_1} for $\alpha \in \{0.4, 0.5, 0.6, 0.7\}$.

QNMs from V_{GD_1}

n	n_0	$\alpha = 0.8$		$\alpha = 0.9$		$\alpha = 1.0$	
		$\text{Re}(\omega)$	$\text{Im}(\omega)$	$\text{Re}(\omega)$	$\text{Im}(\omega)$	$\text{Re}(\omega)$	$\text{Im}(\omega)$
2	0	0.36887	-0.08868	0.36828	-0.08865	0.36768	-0.08863
	1	0.34003	-0.27318	0.33923	-0.27317	0.33843	-0.27315
	2	0.28918	-0.47914	0.28797	-0.47937	0.28674	-0.47962
3	0	0.59544	-0.09244	0.59494	-0.09240	0.59444	-0.09237
	1	0.57811	-0.28048	0.57754	-0.28038	0.57697	-0.28028
	2	0.54584	-0.47774	0.54511	-0.47758	0.54438	-0.47742
	3	0.50317	-0.68897	0.50215	-0.68878	0.50114	-0.68860
4	0	0.80542	-0.09397	0.80495	-0.09395	0.80448	-0.09393
	1	0.79243	-0.28375	0.79191	-0.28367	0.79138	-0.28360
	2	0.76751	-0.47888	0.76686	-0.47876	0.76621	-0.47863
	3	0.73273	-0.68251	0.73185	-0.68235	0.73097	-0.68218
	4	0.69089	-0.89702	0.68965	-0.89686	0.68841	-0.89671
5	0	1.00856	-0.09473	1.00810	-0.09472	1.00763	-0.09470
	1	0.99811	-0.28539	0.99760	-0.28534	0.99709	-0.28529
	2	0.97777	-0.47958	0.97715	-0.47949	0.97653	-0.47940
	3	0.94863	-0.67947	0.94783	-0.67935	0.94704	-0.67922
	4	0.91229	-0.88693	0.91122	-0.88679	0.91014	-0.88665
	5	0.87065	-1.10338	0.86916	-1.10328	0.86767	-1.10319
6	0	1.20819	-0.09516	1.20771	-0.09515	1.20723	-0.09514
	1	1.19943	-0.28633	1.19891	-0.28629	1.19839	-0.28625
	2	1.18223	-0.48000	1.18162	-0.47993	1.18102	-0.47986
	3	1.15725	-0.67775	1.15650	-0.67766	1.15575	-0.67756
	4	1.12547	-0.88104	1.12450	-0.88092	1.12352	-0.88081
	5	1.08810	-1.09105	1.08681	-1.09095	1.08551	-1.09084
	6	1.04650	-1.30876	1.04476	-1.30872	1.04302	-1.30869

TABLE VII: Real and imaginary parts from the QNMs of potential V_{GD_1} for $\alpha \in \{0.8, 0.9, 1.0\}$.

QNMs from V_{GD_2}

n	n_0	$\alpha = 0.0$		$\alpha = 0.1$		$\alpha = 0.2$		$\alpha = 0.3$	
		$\text{Re}(\omega)$	$\text{Im}(\omega)$	$\text{Re}(\omega)$	$\text{Im}(\omega)$	$\text{Re}(\omega)$	$\text{Im}(\omega)$	$\text{Re}(\omega)$	$\text{Im}(\omega)$
2	0	0.37362	-0.08889	0.19256	-0.03387	0.19275	-0.03391	0.19280	-0.03397
	1	0.34630	-0.27348	0.18480	-0.10305	0.18546	-0.10290	0.18487	-0.10348
	2	0.29852	-0.47756	0.17014	-0.17662	0.17248	-0.17453	0.16950	-0.17808
3	0	0.59944	-0.09270	0.30756	-0.03533	0.30778	-0.03537	0.30804	-0.03540
	1	0.58264	-0.28129	0.30274	-0.10647	0.30268	-0.10669	0.30314	-0.10674
	2	0.55159	-0.47905	0.29380	-0.17873	0.29227	-0.18004	0.29366	-0.17957
	3	0.51110	-0.69047	0.28217	-0.25163	0.27610	-0.25774	0.28022	-0.25459
4	0	0.80918	-0.09416	0.41428	-0.03585	0.41462	-0.03588	0.41497	-0.03592
	1	0.79663	-0.28433	0.41049	-0.10787	0.41085	-0.10797	0.41124	-0.10807
	2	0.77270	-0.47990	0.40290	-0.18090	0.40326	-0.18108	0.40382	-0.18118
	3	0.73966	-0.68390	0.39139	-0.25582	0.39167	-0.25617	0.39272	-0.25604
	4	0.70064	-0.89846	0.37572	-0.33398	0.37572	-0.33474	0.37791	-0.33364
5	0	1.01230	-0.09487	0.51772	-0.03609	0.51815	-0.03612	0.51859	-0.03615
	1	1.00222	-0.28582	0.51470	-0.10848	0.51514	-0.10858	0.51560	-0.10867
	2	0.98269	-0.48033	0.50870	-0.18148	0.50909	-0.18166	0.50965	-0.18180
	3	0.95496	-0.68054	0.49980	-0.25550	0.49995	-0.25591	0.50078	-0.25599
	4	0.92081	-0.88819	0.48811	-0.33097	0.48753	-0.33205	0.48899	-0.33178
	5	0.88238	-1.10445	0.47375	-0.40835	0.47150	-0.41122	0.47428	-0.40983
6	0	1.21201	-0.09527	0.61947	-0.03623	0.61999	-0.03625	0.62053	-0.03628
	1	1.20357	-0.28665	0.61694	-0.10882	0.61748	-0.10891	0.61803	-0.10900
	2	1.18707	-0.48056	0.61188	-0.18185	0.61243	-0.18200	0.61307	-0.18213
	3	1.16326	-0.67858	0.60430	-0.25563	0.60481	-0.25589	0.60572	-0.25597
	4	1.13323	-0.88208	0.59417	-0.33054	0.59449	-0.33101	0.59609	-0.33077
	5	1.09837	-1.09213	0.58139	-0.40707	0.58123	-0.40805	0.58432	-0.40676
	6	1.06023	-1.30946	0.56585	-0.48591	0.56468	-0.48803	0.57060	-0.48414

TABLE VIII: Real and imaginary parts from the QNMs of potential V_{GD_2} for $\alpha \in \{0.0, 0.1, 0.2, 0.3\}$.

QNMs from V_{GD_2}

n	n_0	$\alpha = 0.4$		$\alpha = 0.5$		$\alpha = 0.6$		$\alpha = 0.7$	
		$\text{Re}(\omega)$	$\text{Im}(\omega)$	$\text{Re}(\omega)$	$\text{Im}(\omega)$	$\text{Re}(\omega)$	$\text{Im}(\omega)$	$\text{Re}(\omega)$	$\text{Im}(\omega)$
2	0	0.19314	-0.03399	0.19315	-0.03407	0.19327	-0.03412	0.19324	-0.03420
	1	0.18715	-0.10245	0.18595	-0.10333	0.18603	-0.10353	0.18441	-0.10468
	2	0.17937	-0.16866	0.17329	-0.17491	0.17324	-0.17540	0.16552	-0.18401
3	0	0.30828	-0.03544	0.30856	-0.03548	0.30879	-0.03552	0.30904	-0.03556
	1	0.30342	-0.10685	0.30402	-0.10685	0.30412	-0.10702	0.30443	-0.10713
	2	0.29405	-0.17971	0.29617	-0.17881	0.29559	-0.17955	0.29609	-0.17963
	3	0.28090	-0.25458	0.28764	-0.24922	0.28485	-0.25227	0.28589	-0.25198
4	0	0.41531	-0.03595	0.41566	-0.03598	0.41600	-0.03602	0.41635	-0.03605
	1	0.41163	-0.10816	0.41202	-0.10826	0.41236	-0.10837	0.41275	-0.10846
	2	0.40437	-0.18129	0.40492	-0.18140	0.40516	-0.18164	0.40571	-0.18176
	3	0.39374	-0.25592	0.39474	-0.25581	0.39460	-0.25645	0.39558	-0.25637
	4	0.38007	-0.33255	0.38211	-0.33156	0.38090	-0.33341	0.38292	-0.33246
5	0	0.51903	-0.03619	0.51947	-0.03622	0.51991	-0.03625	0.52035	-0.03628
	1	0.51606	-0.10876	0.51653	-0.10885	0.51700	-0.10895	0.51745	-0.10905
	2	0.51016	-0.18195	0.51075	-0.18207	0.51132	-0.18221	0.51177	-0.18239
	3	0.50136	-0.25619	0.50233	-0.25620	0.50317	-0.25628	0.50352	-0.25662
	4	0.48971	-0.33198	0.49159	-0.33143	0.49310	-0.33112	0.49311	-0.33185
	5	0.47523	-0.40994	0.47902	-0.40768	0.48191	-0.40621	0.48110	-0.40790
6	0	0.62106	-0.03631	0.62159	-0.03635	0.62212	-0.03638	0.62265	-0.03641
	1	0.61858	-0.10909	0.61912	-0.10918	0.61966	-0.10927	0.62022	-0.10937
	2	0.61365	-0.18228	0.61365	-0.18228	0.61422	-0.18244	0.61539	-0.18275
	3	0.60636	-0.25618	0.60696	-0.25640	0.60747	-0.25667	0.60824	-0.25684
	4	0.59681	-0.33102	0.59743	-0.33134	0.59773	-0.33183	0.59887	-0.33189
	5	0.58516	-0.40704	0.58575	-0.40751	0.58552	-0.40852	0.58745	-0.40813
	6	0.57160	-0.48439	0.57206	-0.48515	0.57413	-0.48577	0.57413	-0.48577

TABLE IX: Real and imaginary parts from the QNMs of potential V_{GD_2} for $\alpha \in \{0.4, 0.5, 0.6, 0.7\}$.

QNMs from V_{GD_2}

n	n_0	$\alpha = 0.8$		$\alpha = 0.9$		$\alpha = 1.0$	
		$\text{Re}(\omega)$	$\text{Im}(\omega)$	$\text{Re}(\omega)$	$\text{Im}(\omega)$	$\text{Re}(\omega)$	$\text{Im}(\omega)$
2	0	0.19337	-0.03426	0.19369	-0.03428	0.19374	-0.03435
	1	0.18446	-0.10488	0.18661	-0.10393	0.18596	-0.10453
	2	0.16524	-0.18471	0.17432	-0.17555	0.17092	-0.17940
3	0	0.30925	-0.03560	0.30954	-0.03564	0.30978	-0.03568
	1	0.30429	-0.10739	0.30496	-0.10737	0.30517	-0.10752
	2	0.29417	-0.18120	0.29668	-0.18005	0.29664	-0.18048
	3	0.27841	-0.25939	0.28649	-0.25268	0.28560	-0.25410
4	0	0.41670	-0.03609	0.41704	-0.03613	0.41740	-0.03616
	1	0.41310	-0.10857	0.41340	-0.10870	0.41386	-0.10879
	2	0.40604	-0.18197	0.40599	-0.18235	0.40697	-0.18229
	3	0.39577	-0.25681	0.39447	-0.25821	0.39714	-0.25705
	4	0.38265	-0.33351	0.37813	-0.33830	0.38498	-0.33314
5	0	0.52079	-0.03632	0.52124	-0.03635	0.52168	-0.03638
	1	0.51791	-0.10915	0.51839	-0.10925	0.51883	-0.10936
	2	0.51224	-0.18257	0.51285	-0.18270	0.51318	-0.18293
	3	0.50397	-0.25690	0.50499	-0.25691	0.50487	-0.25750
	4	0.49345	-0.33235	0.49549	-0.33173	0.49405	-0.33342
	5	0.48111	-0.40888	0.48532	-0.40637	0.48095	-0.41102
6	0	0.62318	-0.03644	0.62372	-0.03647	0.62426	-0.03651
	1	0.62077	-0.10946	0.62131	-0.10956	0.62187	-0.10966
	2	0.61599	-0.18291	0.61652	-0.18309	0.61712	-0.18325
	3	0.60895	-0.25703	0.60936	-0.25735	0.61004	-0.25757
	4	0.59984	-0.33203	0.59984	-0.33270	0.60069	-0.33293
	5	0.58891	-0.40801	0.58791	-0.40959	0.58907	-0.40971
	6	0.57650	-0.48493	0.57350	-0.48862	0.57520	-0.48838

TABLE X: Real and imaginary parts from the QNMs of potential V_{GD_2} for $\alpha \in \{0.8, 0.9, 1.0\}$.

QNMs from V_{GD_3}

n	n_0	$\alpha = 0.0$		$\alpha = 0.1$		$\alpha = 0.2$		$\alpha = 0.3$	
		$\text{Re}(\omega)$	$\text{Im}(\omega)$	$\text{Re}(\omega)$	$\text{Im}(\omega)$	$\text{Re}(\omega)$	$\text{Im}(\omega)$	$\text{Re}(\omega)$	$\text{Im}(\omega)$
2	0	0.37362	-0.08889	0.24914	-0.05938	0.24921	-0.05951	0.24927	-0.05963
	1	0.34630	-0.27348	0.23076	-0.18269	0.23065	-0.18305	0.23054	-0.18343
	2	0.29852	-0.47756	0.19848	-0.31903	0.19794	-0.31971	0.19738	-0.32039
3	0	0.59944	-0.09270	0.39984	-0.06191	0.40006	-0.06203	0.40027	-0.06214
	1	0.58264	-0.28129	0.38857	-0.18787	0.38872	-0.18822	0.38887	-0.18856
	2	0.55159	-0.47905	0.36774	-0.31996	0.36774	-0.32056	0.36775	-0.32116
	3	0.51110	-0.69047	0.34053	-0.46121	0.34032	-0.46210	0.34010	-0.46300
4	0	0.80918	-0.09416	0.53979	-0.06289	0.54012	-0.06300	0.54046	-0.06312
	1	0.79663	-0.28433	0.53138	-0.18990	0.53166	-0.19024	0.53195	-0.19059
	2	0.77270	-0.47990	0.51532	-0.32051	0.51552	-0.32109	0.51571	-0.32168
	3	0.73966	-0.68390	0.49317	-0.45677	0.49322	-0.45760	0.49327	-0.45843
	4	0.70064	-0.89846	0.46697	-0.60007	0.46683	-0.60118	0.46669	-0.60228
5	0	1.01230	-0.09487	0.67531	-0.06336	0.67575	-0.06347	0.67620	-0.06359
	1	1.00222	-0.28582	0.66856	-0.19089	0.66896	-0.19123	0.66937	-0.19158
	2	0.98269	-0.48033	0.65546	-0.32079	0.65580	-0.32137	0.65613	-0.32195
	3	0.95496	-0.68054	0.63686	-0.45451	0.63708	-0.45533	0.63730	-0.45615
	4	0.92081	-0.88819	0.61395	-0.59319	0.61403	-0.59425	0.61410	-0.59532
	5	0.88238	-1.10445	0.58815	-0.73762	0.58804	-0.73893	0.58793	-0.74025
6	0	1.21201	-0.09527	0.80856	-0.06362	0.80911	-0.06374	0.80966	-0.06385
	1	1.20357	-0.28665	0.80290	-0.19144	0.80342	-0.19179	0.80394	-0.19213
	2	1.18707	-0.48056	0.79184	-0.32095	0.79230	-0.32153	0.79275	-0.32211
	3	1.16326	-0.67858	0.77587	-0.45320	0.77623	-0.45401	0.77659	-0.45483
	4	1.13323	-0.88208	0.75573	-0.58910	0.75597	-0.59016	0.75620	-0.59121
	5	1.09837	-1.09213	0.73234	-0.72938	0.73243	-0.73067	0.73251	-0.73197
	6	1.06023	-1.30946	0.70673	-0.87451	0.70664	-0.87758	0.70653	-0.87758

TABLE XI: Real and imaginary parts from the QNMs of potential V_{GD_3} for $\alpha \in \{0.0, 0.1, 0.2, 0.3\}$.

QNMs from V_{GD_3}

n	n_0	$\alpha = 0.4$		$\alpha = 0.5$		$\alpha = 0.6$		$\alpha = 0.7$	
		$\text{Re}(\omega)$	$\text{Im}(\omega)$	$\text{Re}(\omega)$	$\text{Im}(\omega)$	$\text{Re}(\omega)$	$\text{Im}(\omega)$	$\text{Re}(\omega)$	$\text{Im}(\omega)$
2	0	0.24934	-0.05975	0.24940	-0.05988	0.24946	-0.06000	0.24952	-0.06013
	1	0.23042	-0.18380	0.23031	-0.18418	0.23018	-0.18456	0.23006	-0.18494
	2	0.19681	-0.32109	0.19624	-0.32181	0.19565	-0.32254	0.19506	-0.32328
3	0	0.40048	-0.06225	0.40070	-0.06237	0.40091	-0.06248	0.40112	-0.06260
	1	0.38901	-0.18891	0.38915	-0.18926	0.38929	-0.18961	0.38943	-0.18995
	2	0.36775	-0.32176	0.36775	-0.32236	0.36775	-0.32296	0.36774	-0.32357
	3	0.33988	-0.46390	0.33965	-0.46480	0.33942	-0.46571	0.33919	-0.46661
4	0	0.54079	-0.06323	0.54112	-0.06334	0.54146	-0.06346	0.54179	-0.06357
	1	0.53223	-0.19093	0.53252	-0.19128	0.53280	-0.19162	0.53309	-0.19197
	2	0.51590	-0.32226	0.51608	-0.32284	0.51627	-0.32343	0.51645	-0.32402
	3	0.49331	-0.45927	0.49335	-0.46011	0.49339	-0.46094	0.49342	-0.46178
	4	0.46654	-0.60339	0.46639	-0.60449	0.46623	-0.60560	0.46606	-0.60671
5	0	0.67665	-0.06370	0.67709	-0.06382	0.67754	-0.06393	0.67798	-0.06405
	1	0.66978	-0.19192	0.67018	-0.19227	0.67059	-0.19262	0.67099	-0.19296
	2	0.65646	-0.32253	0.65678	-0.32311	0.65711	-0.32370	0.65744	-0.32428
	3	0.63752	-0.45697	0.63773	-0.45779	0.63794	-0.45861	0.63815	-0.45944
	4	0.61416	-0.59639	0.61422	-0.59746	0.61427	-0.59853	0.61432	-0.59960
	5	0.58780	-0.74157	0.58767	-0.74289	0.58753	-0.74421	0.58738	-0.74554
6	0	0.81021	-0.06397	0.81076	-0.06409	0.81132	-0.06420	0.81187	-0.06432
	1	0.80446	-0.19248	0.80498	-0.19283	0.80550	-0.19318	0.80602	-0.19353
	2	0.79321	-0.32269	0.79366	-0.32327	0.79411	-0.32385	0.79456	-0.32444
	3	0.77695	-0.45565	0.77731	-0.45647	0.77766	-0.45729	0.77801	-0.45811
	4	0.75643	-0.59227	0.75666	-0.59333	0.75688	-0.59439	0.75710	-0.59546
	5	0.73258	-0.73327	0.73264	-0.73457	0.73270	-0.73588	0.73275	-0.73718
	6	0.70641	-0.87912	0.70628	-0.88067	0.70628	-0.88221	0.70600	-0.88376

TABLE XII: Real and imaginary parts from the QNMs of potential V_{GD_3} for $\alpha \in \{0.4, 0.5, 0.6, 0.7\}$.

QNMs from V_{GD_3}

n	n_0	$\alpha = 0.8$		$\alpha = 0.9$		$\alpha = 1.0$	
		$\text{Re}(\omega)$	$\text{Im}(\omega)$	$\text{Re}(\omega)$	$\text{Im}(\omega)$	$\text{Re}(\omega)$	$\text{Im}(\omega)$
2	0	0.24964	-0.06038	0.24964	-0.06038	0.24970	-0.06050
	1	0.22993	-0.18533	0.22980	-0.18572	0.22966	-0.18611
	2	0.19445	-0.32404	0.19383	-0.32482	0.19321	-0.32561
3	0	0.40133	-0.06271	0.40154	-0.06283	0.40176	-0.06294
	1	0.38957	-0.19030	0.38971	-0.19065	0.38985	-0.19101
	2	0.36773	-0.32417	0.36772	-0.32478	0.36771	-0.32539
	3	0.33895	-0.46752	0.33870	-0.46843	0.33845	-0.46935
4	0	0.54212	-0.06369	0.54246	-0.06380	0.54279	-0.06392
	1	0.53337	-0.19232	0.53365	-0.19267	0.53393	-0.19302
	2	0.51663	-0.32461	0.51681	-0.32520	0.51699	-0.32579
	3	0.49345	-0.46263	0.49348	-0.46347	0.49350	-0.46432
	4	0.46588	-0.60782	0.46570	-0.60893	0.46551	-0.61005
5	0	0.67843	-0.06417	0.67887	-0.06428	0.67932	-0.06440
	1	0.67140	-0.19331	0.67180	-0.19366	0.67221	-0.19401
	2	0.65776	-0.32487	0.65808	-0.32545	0.65840	-0.32604
	3	0.63835	-0.46027	0.63855	-0.46110	0.63875	-0.46193
	4	0.61436	-0.60068	0.61440	-0.60175	0.61443	-0.60283
	5	0.58722	-0.74686	0.58705	-0.74819	0.58687	-0.74952
6	0	0.81242	-0.06443	0.81297	-0.06455	0.81352	-0.06467
	1	0.80653	-0.19388	0.80705	-0.19423	0.80757	-0.19458
	2	0.79501	-0.32503	0.79546	-0.32561	0.79591	-0.32620
	3	0.77836	-0.45894	0.77870	-0.45977	0.77905	-0.46060
	4	0.75731	-0.59652	0.75752	-0.59759	0.75773	-0.59867
	5	0.73280	-0.73849	0.73284	-0.73980	0.73286	-0.74112
	6	0.70583	-0.88531	0.70566	-0.88686	0.70548	-0.88841

TABLE XIII: Real and imaginary parts from the QNMs of potential V_{GD_3} for $\alpha \in \{0.8, 0.9, 1.0\}$.

Appendix C: $\Delta\omega$ between GD and RN black holes with same $\{r_+, Q^2\}$

Next we display the obtained values for $\Delta\omega$, computed using Eq. (79) for each pair $\{V_{\text{GD}_i}, V_{\text{RN}_i}\}$, $i \in \{1, 2, 3\}$, which compares the QNMs from the GD potentials with the QNMs from the correspondent RN black holes with same values of outer horizon r_+ and squared charge Q^2 .

QNM difference ($\Delta\omega$) for $\{V_{\text{GD}_1}, V_{\text{RN}_1}\}$

n	n_0	$\alpha = 0.1$		$\alpha = 0.2$		$\alpha = 0.3$	
		$\Delta\text{Re}(\omega)$	$\Delta\text{Im}(\omega)$	$\Delta\text{Re}(\omega)$	$\Delta\text{Im}(\omega)$	$\Delta\text{Re}(\omega)$	$\Delta\text{Im}(\omega)$
2	0	9.46×10^{-4}	8.83×10^{-4}	1.90×10^{-3}	1.76×10^{-3}	2.87×10^{-3}	2.64×10^{-3}
	1	6.35×10^{-5}	2.85×10^{-3}	1.49×10^{-4}	5.68×10^{-3}	2.56×10^{-4}	8.50×10^{-3}
	2	1.62×10^{-3}	5.58×10^{-3}	3.19×10^{-3}	1.11×10^{-2}	4.71×10^{-3}	1.66×10^{-2}
3	0	2.10×10^{-3}	9.22×10^{-4}	4.20×10^{-3}	1.84×10^{-3}	6.32×10^{-3}	2.76×10^{-3}
	1	1.64×10^{-3}	2.84×10^{-3}	3.29×10^{-3}	5.67×10^{-3}	4.97×10^{-3}	8.48×10^{-3}
	2	7.54×10^{-4}	4.98×10^{-3}	1.54×10^{-3}	9.94×10^{-3}	2.35×10^{-3}	1.49×10^{-2}
	3	4.90×10^{-4}	7.50×10^{-3}	9.34×10^{-4}	1.50×10^{-2}	1.33×10^{-3}	2.24×10^{-2}
4	0	3.09×10^{-3}	9.53×10^{-4}	6.20×10^{-3}	1.90×10^{-3}	9.32×10^{-3}	2.85×10^{-3}
	1	2.75×10^{-3}	2.90×10^{-3}	5.51×10^{-3}	5.79×10^{-3}	8.30×10^{-3}	8.67×10^{-3}
	2	2.06×10^{-3}	4.97×10^{-3}	4.16×10^{-3}	9.92×10^{-3}	6.27×10^{-3}	1.49×10^{-2}
	3	1.07×10^{-3}	7.26×10^{-3}	2.17×10^{-3}	1.45×10^{-2}	3.32×10^{-3}	2.17×10^{-2}
	4	2.12×10^{-4}	9.85×10^{-3}	3.68×10^{-4}	1.97×10^{-2}	4.68×10^{-4}	2.94×10^{-2}
5	0	4.03×10^{-3}	9.71×10^{-4}	8.08×10^{-3}	1.94×10^{-3}	1.21×10^{-2}	2.90×10^{-3}
	1	3.75×10^{-3}	2.94×10^{-3}	7.52×10^{-3}	5.87×10^{-3}	1.13×10^{-2}	8.78×10^{-3}
	2	3.19×10^{-3}	4.99×10^{-3}	6.40×10^{-3}	9.95×10^{-3}	9.65×10^{-3}	1.49×10^{-2}
	3	2.36×10^{-3}	7.17×10^{-3}	4.76×10^{-3}	1.43×10^{-2}	7.20×10^{-3}	2.14×10^{-2}
	4	1.28×10^{-3}	9.56×10^{-3}	2.62×10^{-3}	1.91×10^{-2}	4.00×10^{-3}	2.86×10^{-2}
	5	3.21×10^{-5}	1.22×10^{-2}	3.71×10^{-6}	2.44×10^{-2}	1.10×10^{-4}	3.65×10^{-2}
6	0	4.93×10^{-3}	9.81×10^{-4}	9.88×10^{-3}	1.96×10^{-3}	1.49×10^{-2}	2.93×10^{-3}
	1	4.69×10^{-3}	2.96×10^{-3}	9.41×10^{-3}	5.91×10^{-3}	1.41×10^{-2}	8.85×10^{-3}
	2	4.22×10^{-3}	5.00×10^{-3}	8.47×10^{-3}	9.98×10^{-3}	1.27×10^{-2}	1.49×10^{-2}
	3	3.52×10^{-3}	7.14×10^{-3}	7.07×10^{-3}	1.42×10^{-2}	1.07×10^{-2}	2.13×10^{-2}
	4	2.59×10^{-3}	9.41×10^{-3}	5.23×10^{-3}	1.88×10^{-2}	7.92×10^{-3}	2.81×10^{-2}
	5	1.45×10^{-3}	1.19×10^{-2}	2.97×10^{-3}	2.37×10^{-2}	4.55×10^{-3}	3.55×10^{-2}
	6	1.12×10^{-4}	1.46×10^{-2}	3.06×10^{-4}	2.91×10^{-2}	5.80×10^{-4}	4.35×10^{-2}

TABLE XIV: Real and imaginary parts of the difference $\Delta\omega$ between QNMs of potentials V_{GD_1} and V_{RN_1} for $\alpha \in \{0.1, 0.2, 0.3\}$.

QNM difference ($\Delta\omega$) for $\{V_{\text{GD}_1}, V_{\text{RN}_1}\}$

n	n_0	$\alpha = 0.4$		$\alpha = 0.5$		$\alpha = 0.6$	
		$\Delta\text{Re}(\omega)$	$\Delta\text{Im}(\omega)$	$\Delta\text{Re}(\omega)$	$\Delta\text{Im}(\omega)$	$\Delta\text{Re}(\omega)$	$\Delta\text{Im}(\omega)$
2	0	3.84×10^{-3}	3.52×10^{-3}	4.82×10^{-3}	4.39×10^{-3}	5.81×10^{-3}	5.26×10^{-3}
	1	3.82×10^{-4}	1.13×10^{-2}	5.31×10^{-4}	1.41×10^{-2}	7.01×10^{-4}	1.69×10^{-2}
	2	6.19×10^{-3}	2.21×10^{-2}	7.62×10^{-3}	2.75×10^{-2}	9.01×10^{-3}	3.29×10^{-2}
3	0	8.45×10^{-3}	3.67×10^{-3}	1.06×10^{-2}	4.58×10^{-3}	1.27×10^{-2}	5.48×10^{-3}
	1	6.65×10^{-3}	1.13×10^{-2}	8.36×10^{-3}	1.41×10^{-2}	1.01×10^{-2}	1.69×10^{-2}
	2	3.19×10^{-3}	1.98×10^{-2}	4.06×10^{-3}	2.47×10^{-2}	4.96×10^{-3}	2.95×10^{-2}
	3	1.68×10^{-3}	2.98×10^{-2}	1.99×10^{-3}	3.71×10^{-2}	2.24×10^{-3}	4.44×10^{-2}
4	0	1.25×10^{-2}	3.79×10^{-3}	1.56×10^{-2}	4.73×10^{-3}	1.88×10^{-2}	5.67×10^{-3}
	1	1.11×10^{-2}	1.15×10^{-2}	1.39×10^{-2}	1.44×10^{-2}	1.68×10^{-2}	1.72×10^{-2}
	2	8.42×10^{-3}	1.98×10^{-2}	1.06×10^{-2}	2.47×10^{-2}	1.28×10^{-2}	2.95×10^{-2}
	3	4.51×10^{-3}	2.88×10^{-2}	5.74×10^{-3}	3.60×10^{-2}	7.02×10^{-3}	4.30×10^{-2}
	4	5.07×10^{-4}	3.91×10^{-2}	4.91×10^{-4}	4.88×10^{-2}	4.10×10^{-4}	5.84×10^{-2}
5	0	1.62×10^{-2}	3.86×10^{-3}	2.03×10^{-2}	4.82×10^{-3}	2.44×10^{-2}	5.77×10^{-3}
	1	1.51×10^{-2}	1.17×10^{-2}	1.89×10^{-2}	1.46×10^{-2}	2.28×10^{-2}	1.75×10^{-2}
	2	1.29×10^{-2}	1.98×10^{-2}	1.62×10^{-2}	2.47×10^{-2}	1.95×10^{-2}	2.96×10^{-2}
	3	9.68×10^{-3}	2.85×10^{-2}	1.22×10^{-2}	3.56×10^{-2}	1.47×10^{-2}	4.26×10^{-2}
	4	5.44×10^{-3}	3.80×10^{-2}	6.94×10^{-3}	4.74×10^{-2}	8.49×10^{-3}	5.67×10^{-2}
	5	2.86×10^{-4}	4.85×10^{-2}	5.37×10^{-4}	6.05×10^{-2}	8.57×10^{-4}	7.24×10^{-2}
6	0	1.98×10^{-2}	3.90×10^{-3}	2.48×10^{-2}	4.87×10^{-3}	2.99×10^{-2}	5.83×10^{-3}
	1	1.89×10^{-2}	1.18×10^{-2}	2.37×10^{-2}	1.47×10^{-2}	2.85×10^{-2}	1.76×10^{-2}
	2	1.70×10^{-2}	1.99×10^{-2}	2.14×10^{-2}	2.48×10^{-2}	2.57×10^{-2}	2.97×10^{-2}
	3	1.43×10^{-2}	2.84×10^{-2}	1.80×10^{-2}	3.54×10^{-2}	2.17×10^{-2}	4.24×10^{-2}
	4	1.07×10^{-2}	3.74×10^{-2}	1.34×10^{-2}	4.66×10^{-2}	1.63×10^{-2}	5.58×10^{-2}
	5	6.19×10^{-3}	4.72×10^{-2}	7.91×10^{-3}	5.88×10^{-2}	9.69×10^{-3}	7.04×10^{-2}
	6	9.40×10^{-4}	5.78×10^{-2}	1.38×10^{-3}	7.21×10^{-2}	1.91×10^{-3}	8.63×10^{-2}

TABLE XV: Real and imaginary parts of the difference $\Delta\omega$ between QNMs of potentials V_{GD_1} and V_{RN_1} for $\alpha \in \{0.4, 0.5, 0.6\}$.

QNM difference ($\Delta\omega$) for $\{V_{\text{GD}_1}, V_{\text{RN}_1}\}$

n	n_0	$\alpha = 0.7$		$\alpha = 0.8$	
		$\Delta\text{Re}(\omega)$	$\Delta\text{Im}(\omega)$	$\Delta\text{Re}(\omega)$	$\Delta\text{Im}(\omega)$
2	0	6.81×10^{-3}	6.13×10^{-3}	7.82×10^{-3}	6.99×10^{-3}
	1	8.91×10^{-4}	1.97×10^{-2}	1.10×10^{-3}	2.24×10^{-2}
	2	1.04×10^{-2}	3.83×10^{-2}	1.16×10^{-2}	4.36×10^{-2}
3	0	1.49×10^{-2}	6.39×10^{-3}	1.71×10^{-2}	7.28×10^{-3}
	1	1.18×10^{-2}	1.96×10^{-2}	1.36×10^{-2}	2.24×10^{-2}
	2	5.89×10^{-3}	3.44×10^{-2}	6.86×10^{-3}	3.92×10^{-2}
	3	2.45×10^{-3}	5.17×10^{-2}	2.60×10^{-3}	5.89×10^{-2}
4	0	2.19×10^{-2}	6.60×10^{-3}	2.51×10^{-2}	7.52×10^{-3}
	1	1.96×10^{-2}	2.01×10^{-2}	2.25×10^{-2}	2.29×10^{-2}
	2	1.50×10^{-2}	3.44×10^{-2}	1.73×10^{-2}	3.92×10^{-2}
	3	8.33×10^{-3}	5.01×10^{-2}	9.70×10^{-3}	5.71×10^{-2}
	4	2.69×10^{-4}	6.79×10^{-2}	6.16×10^{-5}	7.74×10^{-2}
5	0	2.85×10^{-2}	6.72×10^{-3}	3.27×10^{-2}	7.66×10^{-3}
	1	2.66×10^{-2}	2.03×10^{-2}	3.05×10^{-2}	2.32×10^{-2}
	2	2.29×10^{-2}	3.45×10^{-2}	2.63×10^{-2}	3.93×10^{-2}
	3	1.73×10^{-2}	4.96×10^{-2}	2.00×10^{-2}	5.65×10^{-2}
	4	1.01×10^{-2}	6.60×10^{-2}	1.18×10^{-2}	7.52×10^{-2}
	5	1.25×10^{-3}	8.42×10^{-2}	1.73×10^{-3}	9.60×10^{-2}
6	0	3.49×10^{-2}	6.79×10^{-3}	4.00×10^{-2}	7.74×10^{-3}
	1	3.33×10^{-2}	2.05×10^{-2}	3.81×10^{-2}	2.34×10^{-2}
	2	3.01×10^{-2}	3.46×10^{-2}	3.45×10^{-2}	3.94×10^{-2}
	3	2.54×10^{-2}	4.93×10^{-2}	2.92×10^{-2}	5.62×10^{-2}
	4	1.92×10^{-2}	6.50×10^{-2}	2.21×10^{-2}	7.41×10^{-2}
	5	1.15×10^{-2}	8.19×10^{-2}	1.35×10^{-2}	9.34×10^{-2}
	6	2.53×10^{-3}	1.00×10^{-1}	3.24×10^{-3}	1.15×10^{-1}

TABLE XVI: Real and imaginary parts of the difference $\Delta\omega$ between QNMs of potentials V_{GD_1} and V_{RN_1} for $\alpha \in \{0.7, 0.8\}$.

QNM difference ($\Delta\omega$) for $\{V_{\text{GD}_1}, V_{\text{RN}_1}\}$

n	n_0	$\alpha = 0.9$		$\alpha = 1.0$	
		$\Delta\text{Re}(\omega)$	$\Delta\text{Im}(\omega)$	$\Delta\text{Re}(\omega)$	$\Delta\text{Im}(\omega)$
2	0	8.83×10^{-3}	7.85×10^{-3}	9.86×10^{-3}	8.71×10^{-3}
	1	1.33×10^{-3}	2.52×10^{-2}	1.58×10^{-3}	2.80×10^{-2}
	2	1.29×10^{-2}	4.89×10^{-2}	1.41×10^{-2}	5.42×10^{-2}
3	0	1.92×10^{-2}	8.18×10^{-3}	2.14×10^{-2}	9.07×10^{-3}
	1	1.54×10^{-2}	2.51×10^{-2}	1.71×10^{-2}	2.79×10^{-2}
	2	7.85×10^{-3}	4.40×10^{-2}	8.88×10^{-3}	4.88×10^{-2}
	3	2.71×10^{-3}	6.61×10^{-2}	2.76×10^{-3}	7.32×10^{-2}
4	0	2.83×10^{-2}	8.44×10^{-3}	3.15×10^{-2}	9.36×10^{-3}
	1	2.54×10^{-2}	2.57×10^{-2}	2.83×10^{-2}	2.85×10^{-2}
	2	1.96×10^{-2}	4.40×10^{-2}	2.19×10^{-2}	4.87×10^{-2}
	3	1.11×10^{-2}	6.41×10^{-2}	1.26×10^{-2}	7.10×10^{-2}
	4	2.10×10^{-4}	8.68×10^{-2}	5.34×10^{-4}	9.62×10^{-2}
5	0	3.68×10^{-2}	8.60×10^{-3}	4.10×10^{-2}	9.53×10^{-3}
	1	3.44×10^{-2}	2.60×10^{-2}	3.84×10^{-2}	2.88×10^{-2}
	2	2.97×10^{-2}	4.41×10^{-2}	3.31×10^{-2}	4.89×10^{-2}
	3	2.27×10^{-2}	6.34×10^{-2}	2.54×10^{-2}	7.03×10^{-2}
	4	1.35×10^{-2}	8.44×10^{-2}	1.53×10^{-2}	9.35×10^{-2}
	5	2.28×10^{-3}	1.08×10^{-1}	2.92×10^{-3}	1.19×10^{-1}
6	0	4.50×10^{-2}	8.69×10^{-3}	5.01×10^{-2}	9.63×10^{-3}
	1	4.30×10^{-2}	2.62×10^{-2}	4.79×10^{-2}	2.91×10^{-2}
	2	3.90×10^{-2}	4.42×10^{-2}	4.35×10^{-2}	4.90×10^{-2}
	3	3.30×10^{-2}	6.31×10^{-2}	3.69×10^{-2}	6.99×10^{-2}
	4	2.52×10^{-2}	8.31×10^{-2}	2.82×10^{-2}	9.21×10^{-2}
	5	1.55×10^{-2}	1.05×10^{-1}	1.75×10^{-2}	1.16×10^{-1}
	6	4.04×10^{-3}	1.28×10^{-1}	4.94×10^{-3}	1.42×10^{-1}

TABLE XVII: Real and imaginary parts of the difference $\Delta\omega$ between QNMs of potentials V_{GD_1} and V_{RN_1} for $\alpha \in \{0.9, 1.0\}$.

QNM difference ($\Delta\omega$) for $\{V_{\text{GD}_2}, V_{\text{RN}_2}\}$

n	n_0	$\alpha = 0.1$		$\alpha = 0.2$		$\alpha = 0.3$	
		$\Delta\text{Re}(\omega)$	$\Delta\text{Im}(\omega)$	$\Delta\text{Re}(\omega)$	$\Delta\text{Im}(\omega)$	$\Delta\text{Re}(\omega)$	$\Delta\text{Im}(\omega)$
2	0	5.17×10^{-4}	1.49×10^{-5}	2.30×10^{-4}	2.13×10^{-4}	1.08×10^{-5}	4.38×10^{-4}
	1	4.26×10^{-3}	2.17×10^{-3}	1.91×10^{-3}	2.55×10^{-4}	1.58×10^{-4}	1.32×10^{-3}
	2	1.75×10^{-2}	1.97×10^{-2}	8.05×10^{-3}	6.96×10^{-3}	4.72×10^{-4}	2.24×10^{-3}
3	0	2.98×10^{-4}	3.03×10^{-5}	1.75×10^{-4}	2.14×10^{-4}	5.32×10^{-5}	4.02×10^{-4}
	1	9.07×10^{-4}	1.14×10^{-4}	4.57×10^{-4}	5.76×10^{-4}	7.65×10^{-5}	1.26×10^{-3}
	2	3.85×10^{-3}	1.98×10^{-3}	1.59×10^{-3}	3.74×10^{-4}	2.75×10^{-4}	2.52×10^{-3}
	3	1.26×10^{-2}	1.11×10^{-2}	4.73×10^{-3}	2.25×10^{-3}	1.88×10^{-3}	5.46×10^{-3}
4	0	3.35×10^{-4}	3.24×10^{-5}	2.35×10^{-4}	2.09×10^{-4}	1.29×10^{-4}	3.90×10^{-4}
	1	2.63×10^{-4}	1.21×10^{-4}	2.63×10^{-4}	6.40×10^{-4}	2.52×10^{-4}	1.17×10^{-3}
	2	1.92×10^{-4}	4.25×10^{-4}	1.48×10^{-4}	1.19×10^{-3}	4.44×10^{-4}	2.00×10^{-3}
	3	1.84×10^{-3}	1.72×10^{-3}	5.61×10^{-4}	2.29×10^{-3}	5.49×10^{-4}	3.03×10^{-3}
	4	6.06×10^{-3}	6.05×10^{-3}	2.64×10^{-3}	5.12×10^{-3}	2.84×10^{-4}	4.69×10^{-3}
5	0	4.34×10^{-4}	2.98×10^{-5}	3.12×10^{-4}	2.05×10^{-4}	1.84×10^{-4}	3.85×10^{-4}
	1	4.34×10^{-4}	9.30×10^{-5}	3.43×10^{-4}	6.23×10^{-4}	2.59×10^{-4}	1.16×10^{-3}
	2	3.72×10^{-4}	1.90×10^{-4}	2.83×10^{-4}	1.11×10^{-3}	2.59×10^{-4}	2.02×10^{-3}
	3	6.85×10^{-5}	4.49×10^{-4}	2.25×10^{-4}	1.91×10^{-3}	2.58×10^{-4}	3.28×10^{-3}
	4	8.25×10^{-4}	1.24×10^{-3}	1.88×10^{-3}	3.77×10^{-3}	2.17×10^{-3}	5.83×10^{-3}
	5	2.83×10^{-3}	3.35×10^{-3}	5.74×10^{-3}	8.28×10^{-3}	6.81×10^{-3}	1.17×10^{-2}
6	0	5.25×10^{-4}	2.86×10^{-5}	3.87×10^{-4}	2.03×10^{-4}	2.40×10^{-4}	3.82×10^{-4}
	1	5.34×10^{-4}	8.68×10^{-5}	4.41×10^{-4}	6.10×10^{-4}	3.39×10^{-4}	1.15×10^{-3}
	2	5.27×10^{-4}	1.56×10^{-4}	5.43×10^{-4}	1.02×10^{-3}	5.33×10^{-4}	1.91×10^{-3}
	3	4.29×10^{-4}	2.79×10^{-4}	6.65×10^{-4}	1.45×10^{-3}	7.98×10^{-4}	2.69×10^{-3}
	4	8.36×10^{-5}	5.86×10^{-4}	7.44×10^{-4}	1.95×10^{-3}	1.07×10^{-3}	3.54×10^{-3}
	5	7.68×10^{-4}	1.37×10^{-3}	6.74×10^{-4}	2.64×10^{-3}	1.25×10^{-3}	4.55×10^{-3}
	6	2.47×10^{-3}	3.20×10^{-3}	3.09×10^{-4}	3.75×10^{-3}	1.18×10^{-3}	5.97×10^{-3}

TABLE XVIII: Real and imaginary parts of the difference $\Delta\omega$ between QNMs of potentials V_{GD_2} and V_{RN_2} for $\alpha \in \{0.1, 0.2, 0.3\}$.

QNM difference ($\Delta\omega$) for $\{V_{\text{GD}_2}, V_{\text{RN}_2}\}$

n	n_0	$\alpha = 0.4$		$\alpha = 0.5$		$\alpha = 0.6$	
		$\Delta\text{Re}(\omega)$	$\Delta\text{Im}(\omega)$	$\Delta\text{Re}(\omega)$	$\Delta\text{Im}(\omega)$	$\Delta\text{Re}(\omega)$	$\Delta\text{Im}(\omega)$
2	0	8.11×10^{-5}	6.08×10^{-4}	1.11×10^{-4}	7.94×10^{-4}	2.03×10^{-4}	1.04×10^{-3}
	1	1.93×10^{-3}	9.30×10^{-4}	3.13×10^{-3}	8.76×10^{-4}	6.06×10^{-4}	2.88×10^{-3}
	2	8.72×10^{-3}	4.82×10^{-3}	1.38×10^{-2}	9.87×10^{-3}	2.74×10^{-3}	3.21×10^{-3}
3	0	2.61×10^{-5}	5.89×10^{-4}	8.84×10^{-5}	7.78×10^{-4}	2.40×10^{-4}	9.82×10^{-4}
	1	2.49×10^{-4}	1.76×10^{-3}	6.66×10^{-4}	2.18×10^{-3}	6.95×10^{-5}	2.97×10^{-3}
	2	9.12×10^{-4}	2.83×10^{-3}	3.42×10^{-3}	2.33×10^{-3}	3.31×10^{-4}	5.25×10^{-3}
	3	2.18×10^{-3}	3.52×10^{-3}	1.08×10^{-2}	2.60×10^{-3}	3.41×10^{-4}	8.91×10^{-3}
4	0	1.17×10^{-5}	5.76×10^{-4}	1.10×10^{-4}	7.67×10^{-4}	2.21×10^{-4}	9.61×10^{-4}
	1	1.62×10^{-4}	1.74×10^{-3}	8.98×10^{-5}	2.32×10^{-3}	2.31×10^{-4}	2.85×10^{-3}
	2	2.78×10^{-4}	3.03×10^{-3}	2.22×10^{-4}	4.04×10^{-3}	1.45×10^{-3}	4.50×10^{-3}
	3	1.40×10^{-4}	4.91×10^{-3}	4.51×10^{-4}	6.59×10^{-3}	4.22×10^{-3}	5.13×10^{-3}
	4	1.99×10^{-3}	8.64×10^{-3}	3.27×10^{-3}	1.18×10^{-2}	9.78×10^{-3}	2.72×10^{-3}
5	0	5.50×10^{-5}	5.69×10^{-4}	8.87×10^{-5}	7.59×10^{-4}	2.38×10^{-4}	9.54×10^{-4}
	1	2.56×10^{-4}	1.70×10^{-3}	1.56×10^{-4}	2.27×10^{-3}	7.61×10^{-5}	2.85×10^{-3}
	2	7.54×10^{-4}	2.78×10^{-3}	6.86×10^{-4}	3.75×10^{-3}	7.56×10^{-4}	4.70×10^{-3}
	3	1.81×10^{-3}	3.61×10^{-3}	1.59×10^{-3}	5.12×10^{-3}	1.91×10^{-3}	6.38×10^{-3}
	4	3.89×10^{-3}	3.67×10^{-3}	3.01×10^{-3}	6.21×10^{-3}	3.74×10^{-3}	7.66×10^{-3}
	5	7.68×10^{-3}	1.86×10^{-3}	5.14×10^{-3}	6.67×10^{-3}	6.50×10^{-3}	8.06×10^{-3}
6	0	8.44×10^{-5}	5.66×10^{-4}	8.15×10^{-5}	7.55×10^{-4}	2.57×10^{-4}	9.50×10^{-4}
	1	2.39×10^{-4}	1.70×10^{-3}	1.15×10^{-4}	2.26×10^{-3}	1.01×10^{-5}	2.85×10^{-3}
	2	5.70×10^{-4}	2.81×10^{-3}	4.91×10^{-4}	3.77×10^{-3}	4.42×10^{-4}	4.74×10^{-3}
	3	1.13×10^{-3}	3.88×10^{-3}	9.84×10^{-4}	5.30×10^{-3}	9.60×10^{-4}	6.70×10^{-3}
	4	2.00×10^{-3}	4.82×10^{-3}	1.44×10^{-3}	6.97×10^{-3}	1.23×10^{-3}	8.96×10^{-3}
	5	3.33×10^{-3}	5.45×10^{-3}	1.58×10^{-3}	9.06×10^{-3}	6.98×10^{-4}	1.21×10^{-2}
	6	5.29×10^{-3}	5.47×10^{-3}	1.03×10^{-3}	1.21×10^{-2}	1.39×10^{-3}	1.72×10^{-2}

TABLE XIX: Real and imaginary parts of the difference $\Delta\omega$ between QNMs of potentials V_{GD_2} and V_{RN_2} for $\alpha \in \{0.4, 0.5, 0.6\}$.

QNM difference ($\Delta\omega$) for $\{V_{\text{GD}_2}, V_{\text{RN}_2}\}$

n	n_0	$\alpha = 0.7$		$\alpha = 0.8$	
		$\Delta\text{Re}(\omega)$	$\Delta\text{Im}(\omega)$	$\Delta\text{Re}(\omega)$	$\Delta\text{Im}(\omega)$
2	0	1.32×10^{-3}	1.39×10^{-3}	1.51×10^{-3}	1.59×10^{-3}
	1	4.68×10^{-4}	3.80×10^{-3}	5.29×10^{-4}	4.43×10^{-3}
	2	4.16×10^{-3}	7.12×10^{-3}	4.80×10^{-3}	8.32×10^{-3}
3	0	2.98×10^{-3}	1.34×10^{-3}	3.40×10^{-3}	1.54×10^{-3}
	1	2.27×10^{-3}	4.11×10^{-3}	2.59×10^{-3}	4.70×10^{-3}
	2	8.49×10^{-4}	7.15×10^{-3}	9.61×10^{-4}	8.17×10^{-3}
	3	1.27×10^{-3}	1.07×10^{-2}	1.47×10^{-3}	1.22×10^{-2}
4	0	4.38×10^{-3}	1.36×10^{-3}	5.00×10^{-3}	1.55×10^{-3}
	1	3.87×10^{-3}	4.12×10^{-3}	4.42×10^{-3}	4.71×10^{-3}
	2	2.87×10^{-3}	7.01×10^{-3}	3.27×10^{-3}	8.01×10^{-3}
	3	1.41×10^{-3}	1.01×10^{-2}	1.60×10^{-3}	1.16×10^{-2}
	4	4.70×10^{-4}	1.35×10^{-2}	5.63×10^{-4}	1.54×10^{-2}
5	0	5.69×10^{-3}	1.37×10^{-3}	6.50×10^{-3}	1.57×10^{-3}
	1	5.28×10^{-3}	4.13×10^{-3}	6.04×10^{-3}	4.73×10^{-3}
	2	4.48×10^{-3}	6.97×10^{-3}	5.12×10^{-3}	7.97×10^{-3}
	3	3.31×10^{-3}	9.93×10^{-3}	3.77×10^{-3}	1.14×10^{-2}
	4	1.78×10^{-3}	1.30×10^{-2}	2.02×10^{-3}	1.49×10^{-2}
	5	6.55×10^{-5}	1.63×10^{-2}	1.05×10^{-4}	1.87×10^{-2}
6	0	6.96×10^{-3}	1.38×10^{-3}	7.95×10^{-3}	1.57×10^{-3}
	1	6.62×10^{-3}	4.15×10^{-3}	7.56×10^{-3}	4.74×10^{-3}
	2	5.94×10^{-3}	6.97×10^{-3}	6.79×10^{-3}	7.97×10^{-3}
	3	4.94×10^{-3}	9.87×10^{-3}	5.64×10^{-3}	1.13×10^{-2}
	4	3.65×10^{-3}	1.29×10^{-2}	4.15×10^{-3}	1.47×10^{-2}
	5	2.06×10^{-3}	1.60×10^{-2}	2.33×10^{-3}	1.83×10^{-2}
	6	2.09×10^{-4}	1.92×10^{-2}	2.00×10^{-4}	2.19×10^{-2}

TABLE XX: Real and imaginary parts of the difference $\Delta\omega$ between QNMs of potentials V_{GD_2} and V_{RN_2} for $\alpha \in \{0.7, 0.8\}$.

QNM difference ($\Delta\omega$) for $\{V_{\text{GD}_2}, V_{\text{RN}_2}\}$

n	n_0	$\alpha = 0.9$		$\alpha = 1.0$	
		$\Delta\text{Re}(\omega)$	$\Delta\text{Im}(\omega)$	$\Delta\text{Re}(\omega)$	$\Delta\text{Im}(\omega)$
2	0	2.42×10^{-4}	1.66×10^{-3}	5.14×10^{-4}	1.92×10^{-3}
	1	2.88×10^{-3}	3.59×10^{-3}	9.24×10^{-4}	5.33×10^{-3}
	2	1.28×10^{-2}	3.81×10^{-3}	4.14×10^{-3}	6.50×10^{-3}
3	0	4.66×10^{-4}	1.60×10^{-3}	5.87×10^{-4}	1.82×10^{-3}
	1	1.35×10^{-3}	4.37×10^{-3}	1.33×10^{-3}	5.03×10^{-3}
	2	8.03×10^{-3}	3.91×10^{-3}	8.12×10^{-3}	5.03×10^{-3}
	3	2.55×10^{-2}	9.97×10^{-3}	2.55×10^{-2}	8.17×10^{-3}
4	0	6.47×10^{-4}	1.58×10^{-3}	7.76×10^{-4}	1.80×10^{-3}
	1	4.64×10^{-5}	4.72×10^{-3}	1.95×10^{-4}	5.29×10^{-3}
	2	1.00×10^{-3}	7.83×10^{-3}	2.86×10^{-3}	8.11×10^{-3}
	3	2.05×10^{-3}	1.12×10^{-2}	9.07×10^{-3}	8.34×10^{-3}
	4	2.28×10^{-3}	1.58×10^{-2}	2.18×10^{-2}	9.05×10^{-4}
5	0	7.37×10^{-4}	1.57×10^{-3}	9.19×10^{-4}	1.79×10^{-3}
	1	1.81×10^{-4}	4.69×10^{-3}	2.61×10^{-4}	5.33×10^{-3}
	2	9.99×10^{-4}	7.68×10^{-3}	1.15×10^{-3}	8.70×10^{-3}
	3	2.97×10^{-3}	1.04×10^{-2}	3.59×10^{-3}	1.16×10^{-2}
	4	6.00×10^{-3}	1.23×10^{-2}	7.52×10^{-3}	1.34×10^{-2}
	5	1.05×10^{-2}	1.28×10^{-2}	1.36×10^{-2}	1.29×10^{-2}
6	0	8.40×10^{-4}	1.57×10^{-3}	1.06×10^{-3}	1.78×10^{-3}
	1	3.88×10^{-4}	4.68×10^{-3}	5.21×10^{-4}	5.33×10^{-3}
	2	4.92×10^{-4}	7.75×10^{-3}	5.34×10^{-4}	8.79×10^{-3}
	3	1.71×10^{-3}	1.08×10^{-2}	2.05×10^{-3}	1.21×10^{-2}
	4	3.04×10^{-3}	1.38×10^{-2}	3.89×10^{-3}	1.54×10^{-2}
	5	4.10×10^{-3}	1.73×10^{-2}	5.80×10^{-3}	1.87×10^{-2}
	6	4.34×10^{-3}	2.19×10^{-2}	7.41×10^{-3}	2.25×10^{-2}

TABLE XXI: Real and imaginary parts of the difference $\Delta\omega$ between QNMs of potentials V_{GD_2} and V_{RN_2} for $\alpha \in \{0.9, 1.0\}$.

QNM difference ($\Delta\omega$) for $\{V_{\text{GD}_3}, V_{\text{RN}_3}\}$

n	n_0	$\alpha = 0.1$		$\alpha = 0.2$		$\alpha = 0.3$	
		$\Delta\text{Re}(\omega)$	$\Delta\text{Im}(\omega)$	$\Delta\text{Re}(\omega)$	$\Delta\text{Im}(\omega)$	$\Delta\text{Re}(\omega)$	$\Delta\text{Im}(\omega)$
2	0	1.91×10^{-4}	1.97×10^{-4}	3.81×10^{-4}	3.94×10^{-4}	5.71×10^{-4}	5.92×10^{-4}
	1	5.09×10^{-4}	2.50×10^{-3}	4.71×10^{-4}	3.10×10^{-3}	2.57×10^{-4}	1.34×10^{-3}
	2	8.88×10^{-4}	4.64×10^{-3}	1.47×10^{-3}	5.75×10^{-3}	1.67×10^{-3}	2.46×10^{-3}
3	0	4.26×10^{-4}	1.91×10^{-4}	8.52×10^{-4}	3.83×10^{-4}	1.28×10^{-3}	5.74×10^{-4}
	1	3.26×10^{-4}	5.85×10^{-4}	6.52×10^{-4}	1.17×10^{-3}	9.77×10^{-4}	1.76×10^{-3}
	2	1.28×10^{-4}	1.02×10^{-3}	2.54×10^{-4}	2.04×10^{-3}	3.77×10^{-4}	3.06×10^{-3}
	3	1.68×10^{-4}	1.53×10^{-3}	3.39×10^{-4}	3.05×10^{-3}	5.16×10^{-4}	4.58×10^{-3}
4	0	6.26×10^{-4}	1.93×10^{-4}	1.25×10^{-3}	3.86×10^{-4}	1.88×10^{-3}	5.80×10^{-4}
	1	5.55×10^{-4}	5.86×10^{-4}	1.11×10^{-3}	1.17×10^{-3}	1.66×10^{-3}	1.76×10^{-3}
	2	4.15×10^{-4}	9.97×10^{-4}	8.28×10^{-4}	2.00×10^{-3}	1.24×10^{-3}	3.00×10^{-3}
	3	2.12×10^{-4}	1.44×10^{-3}	4.20×10^{-4}	2.88×10^{-3}	6.25×10^{-4}	4.32×10^{-3}
	4	4.90×10^{-5}	1.92×10^{-3}	1.04×10^{-4}	3.85×10^{-3}	1.65×10^{-4}	5.77×10^{-3}
5	0	8.13×10^{-4}	1.95×10^{-4}	1.63×10^{-3}	3.89×10^{-4}	2.44×10^{-3}	5.85×10^{-4}
	1	7.56×10^{-4}	5.88×10^{-4}	1.51×10^{-3}	1.18×10^{-3}	2.27×10^{-3}	1.77×10^{-3}
	2	6.44×10^{-4}	9.92×10^{-4}	1.29×10^{-3}	1.99×10^{-3}	1.93×10^{-3}	2.98×10^{-3}
	3	4.80×10^{-4}	1.41×10^{-3}	9.58×10^{-4}	2.83×10^{-3}	1.43×10^{-3}	4.25×10^{-3}
	4	2.69×10^{-4}	1.86×10^{-3}	5.34×10^{-4}	3.72×10^{-3}	7.93×10^{-4}	5.58×10^{-3}
	5	1.44×10^{-5}	2.33×10^{-3}	2.12×10^{-5}	4.66×10^{-3}	1.89×10^{-5}	6.99×10^{-3}
6	0	9.93×10^{-4}	1.96×10^{-4}	1.99×10^{-3}	3.92×10^{-4}	2.98×10^{-3}	5.88×10^{-4}
	1	9.46×10^{-4}	5.89×10^{-4}	1.89×10^{-3}	1.18×10^{-3}	2.84×10^{-3}	1.77×10^{-3}
	2	8.51×10^{-4}	9.91×10^{-4}	1.70×10^{-3}	1.98×10^{-3}	2.55×10^{-3}	2.98×10^{-3}
	3	7.13×10^{-4}	1.40×10^{-3}	1.42×10^{-3}	2.81×10^{-3}	2.13×10^{-3}	4.22×10^{-3}
	4	5.33×10^{-4}	1.83×10^{-3}	1.06×10^{-3}	3.67×10^{-3}	1.59×10^{-3}	5.50×10^{-3}
	5	3.14×10^{-4}	2.28×10^{-3}	6.21×10^{-4}	4.56×10^{-3}	9.22×10^{-4}	6.84×10^{-3}
	6	5.93×10^{-5}	2.74×10^{-3}	1.07×10^{-4}	5.48×10^{-3}	1.47×10^{-4}	8.22×10^{-3}

TABLE XXII: Real and imaginary parts of the difference $\Delta\omega$ between QNMs of potentials V_{GD_3} and V_{RN_3} for $\alpha \in \{0.1, 0.2, 0.3\}$.

QNM difference ($\Delta\omega$) for $\{V_{\text{GD}_3}, V_{\text{RN}_3}\}$

n	n_0	$\alpha = 0.4$		$\alpha = 0.5$		$\alpha = 0.6$	
		$\Delta\text{Re}(\omega)$	$\Delta\text{Im}(\omega)$	$\Delta\text{Re}(\omega)$	$\Delta\text{Im}(\omega)$	$\Delta\text{Re}(\omega)$	$\Delta\text{Im}(\omega)$
2	0	7.60×10^{-4}	7.90×10^{-4}	9.48×10^{-4}	9.89×10^{-4}	1.14×10^{-3}	1.19×10^{-3}
	1	3.05×10^{-4}	1.95×10^{-3}	3.56×10^{-4}	2.57×10^{-3}	4.10×10^{-4}	3.18×10^{-3}
	2	2.28×10^{-3}	3.61×10^{-3}	2.90×10^{-3}	4.76×10^{-3}	3.52×10^{-3}	5.94×10^{-3}
3	0	1.70×10^{-3}	7.66×10^{-4}	2.13×10^{-3}	9.58×10^{-4}	2.55×10^{-3}	1.15×10^{-3}
	1	1.30×10^{-3}	2.35×10^{-3}	1.62×10^{-3}	2.93×10^{-3}	1.95×10^{-3}	3.52×10^{-3}
	2	4.98×10^{-4}	4.08×10^{-3}	6.17×10^{-4}	5.10×10^{-3}	7.35×10^{-4}	6.12×10^{-3}
	3	6.97×10^{-4}	6.11×10^{-3}	8.84×10^{-4}	7.64×10^{-3}	1.07×10^{-3}	9.17×10^{-3}
4	0	2.50×10^{-3}	7.74×10^{-4}	3.13×10^{-3}	9.68×10^{-4}	3.75×10^{-3}	1.16×10^{-3}
	1	2.21×10^{-3}	2.35×10^{-3}	2.77×10^{-3}	2.94×10^{-3}	3.32×10^{-3}	3.53×10^{-3}
	2	1.65×10^{-3}	4.00×10^{-3}	2.06×10^{-3}	5.00×10^{-3}	2.47×10^{-3}	6.00×10^{-3}
	3	8.26×10^{-4}	5.77×10^{-3}	1.03×10^{-3}	7.21×10^{-3}	1.22×10^{-3}	8.66×10^{-3}
	4	2.34×10^{-4}	7.70×10^{-3}	3.06×10^{-4}	9.63×10^{-3}	3.85×10^{-4}	1.16×10^{-2}
5	0	3.25×10^{-3}	7.80×10^{-4}	4.06×10^{-3}	9.76×10^{-4}	4.88×10^{-3}	1.17×10^{-3}
	1	3.02×10^{-3}	2.36×10^{-3}	3.78×10^{-3}	2.95×10^{-3}	4.53×10^{-3}	3.54×10^{-3}
	2	2.57×10^{-3}	3.98×10^{-3}	3.21×10^{-3}	4.97×10^{-3}	3.85×10^{-3}	5.97×10^{-3}
	3	1.91×10^{-3}	5.67×10^{-3}	2.38×10^{-3}	7.09×10^{-3}	2.84×10^{-3}	8.51×10^{-3}
	4	1.05×10^{-3}	7.45×10^{-3}	1.30×10^{-3}	9.31×10^{-3}	1.54×10^{-3}	1.12×10^{-2}
	5	9.70×10^{-6}	9.32×10^{-3}	5.69×10^{-6}	1.16×10^{-2}	3.16×10^{-5}	1.40×10^{-2}
6	0	3.97×10^{-3}	7.84×10^{-4}	4.97×10^{-3}	9.81×10^{-4}	5.96×10^{-3}	1.18×10^{-3}
	1	3.78×10^{-3}	2.36×10^{-3}	4.73×10^{-3}	2.96×10^{-3}	5.67×10^{-3}	3.55×10^{-3}
	2	3.40×10^{-3}	3.97×10^{-3}	4.25×10^{-3}	4.97×10^{-3}	5.09×10^{-3}	5.97×10^{-3}
	3	2.84×10^{-3}	5.63×10^{-3}	3.54×10^{-3}	7.04×10^{-3}	4.24×10^{-3}	8.45×10^{-3}
	4	2.11×10^{-3}	7.34×10^{-3}	2.62×10^{-3}	9.18×10^{-3}	3.14×10^{-3}	1.10×10^{-2}
	5	1.44×10^{-3}	1.01×10^{-2}	1.51×10^{-3}	1.14×10^{-2}	1.79×10^{-3}	1.37×10^{-2}
	6	3.28×10^{-4}	1.22×10^{-2}	1.99×10^{-4}	1.37×10^{-2}	2.09×10^{-4}	1.65×10^{-2}

TABLE XXIII: Real and imaginary parts of the difference $\Delta\omega$ between QNMs of potentials V_{GD_1} and V_{RN_1} for $\alpha \in \{0.4, 0.5, 0.6\}$.

QNM difference ($\Delta\omega$) for $\{V_{\text{GD}_3}, V_{\text{RN}_3}\}$

n	n_0	$\alpha = 0.7$		$\alpha = 0.8$	
		$\Delta\text{Re}(\omega)$	$\Delta\text{Im}(\omega)$	$\Delta\text{Re}(\omega)$	$\Delta\text{Im}(\omega)$
2	0	1.32×10^{-3}	1.39×10^{-3}	1.51×10^{-3}	1.59×10^{-3}
	1	4.68×10^{-4}	3.80×10^{-3}	5.29×10^{-4}	4.43×10^{-3}
	2	4.16×10^{-3}	7.12×10^{-3}	4.80×10^{-3}	8.32×10^{-3}
3	0	2.98×10^{-3}	1.34×10^{-3}	3.40×10^{-3}	1.54×10^{-3}
	1	2.27×10^{-3}	4.11×10^{-3}	2.59×10^{-3}	4.70×10^{-3}
	2	8.49×10^{-4}	7.15×10^{-3}	9.61×10^{-4}	8.17×10^{-3}
	3	1.27×10^{-3}	1.07×10^{-2}	1.47×10^{-3}	1.22×10^{-2}
4	0	4.38×10^{-3}	1.36×10^{-3}	5.00×10^{-3}	1.55×10^{-3}
	1	3.87×10^{-3}	4.12×10^{-3}	4.42×10^{-3}	4.71×10^{-3}
	2	2.87×10^{-3}	7.01×10^{-3}	3.27×10^{-3}	8.01×10^{-3}
	3	1.41×10^{-3}	1.01×10^{-2}	1.60×10^{-3}	1.16×10^{-2}
	4	4.70×10^{-4}	1.35×10^{-2}	5.63×10^{-4}	1.54×10^{-2}
5	0	5.69×10^{-3}	1.37×10^{-3}	6.50×10^{-3}	1.57×10^{-3}
	1	5.28×10^{-3}	4.13×10^{-3}	6.04×10^{-3}	4.73×10^{-3}
	2	4.48×10^{-3}	6.97×10^{-3}	5.12×10^{-3}	7.97×10^{-3}
	3	3.31×10^{-3}	9.93×10^{-3}	3.77×10^{-3}	1.14×10^{-2}
	4	1.78×10^{-3}	1.30×10^{-2}	2.02×10^{-3}	1.49×10^{-2}
	5	6.55×10^{-5}	1.63×10^{-2}	1.05×10^{-4}	1.87×10^{-2}
6	0	6.96×10^{-3}	1.38×10^{-3}	7.95×10^{-3}	1.57×10^{-3}
	1	6.62×10^{-3}	4.15×10^{-3}	7.56×10^{-3}	4.74×10^{-3}
	2	5.94×10^{-3}	6.97×10^{-3}	6.79×10^{-3}	7.97×10^{-3}
	3	4.94×10^{-3}	9.87×10^{-3}	5.64×10^{-3}	1.13×10^{-2}
	4	3.65×10^{-3}	1.29×10^{-2}	4.15×10^{-3}	1.47×10^{-2}
	5	2.06×10^{-3}	1.60×10^{-2}	2.33×10^{-3}	1.83×10^{-2}
	6	2.09×10^{-4}	1.92×10^{-2}	2.00×10^{-4}	2.19×10^{-2}

TABLE XXIV: Real and imaginary parts of the difference $\Delta\omega$ between QNMs of potentials V_{GD_3} and V_{RN_3} for $\alpha \in \{0.7, 0.8\}$.

QNM difference ($\Delta\omega$) for $\{V_{\text{GD}_3}, V_{\text{RN}_3}\}$

n	n_0	$\alpha = 0.9$		$\alpha = 1.0$	
		$\Delta\text{Re}(\omega)$	$\Delta\text{Im}(\omega)$	$\Delta\text{Re}(\omega)$	$\Delta\text{Im}(\omega)$
2	0	1.69×10^{-3}	1.79×10^{-3}	1.88×10^{-3}	1.99×10^{-3}
	1	5.93×10^{-4}	5.05×10^{-3}	6.60×10^{-4}	5.68×10^{-3}
	2	5.46×10^{-3}	9.54×10^{-3}	6.12×10^{-3}	1.08×10^{-2}
3	0	3.83×10^{-3}	1.73×10^{-3}	4.25×10^{-3}	1.92×10^{-3}
	1	2.91×10^{-3}	5.29×10^{-3}	3.23×10^{-3}	5.88×10^{-3}
	2	1.07×10^{-3}	9.20×10^{-3}	1.18×10^{-3}	1.02×10^{-2}
	3	1.67×10^{-3}	1.38×10^{-2}	1.88×10^{-3}	1.53×10^{-2}
4	0	5.63×10^{-3}	1.75×10^{-3}	6.25×10^{-3}	1.94×10^{-3}
	1	4.97×10^{-3}	5.30×10^{-3}	5.52×10^{-3}	5.89×10^{-3}
	2	3.68×10^{-3}	9.02×10^{-3}	4.08×10^{-3}	1.00×10^{-2}
	3	1.79×10^{-3}	1.30×10^{-2}	1.97×10^{-3}	1.45×10^{-2}
	4	6.59×10^{-4}	1.73×10^{-2}	7.65×10^{-4}	1.93×10^{-2}
5	0	7.32×10^{-3}	1.76×10^{-3}	8.13×10^{-3}	1.96×10^{-3}
	1	6.79×10^{-3}	5.32×10^{-3}	7.54×10^{-3}	5.92×10^{-3}
	2	5.75×10^{-3}	8.98×10^{-3}	6.39×10^{-3}	9.98×10^{-3}
	3	4.23×10^{-3}	1.28×10^{-2}	4.69×10^{-3}	1.42×10^{-2}
	4	2.25×10^{-3}	1.68×10^{-2}	2.48×10^{-3}	1.87×10^{-2}
	5	1.54×10^{-4}	2.10×10^{-2}	2.12×10^{-4}	2.33×10^{-2}
6	0	8.94×10^{-3}	1.77×10^{-3}	9.94×10^{-3}	1.97×10^{-3}
	1	8.50×10^{-3}	5.34×10^{-3}	9.45×10^{-3}	5.94×10^{-3}
	2	7.63×10^{-3}	8.97×10^{-3}	8.47×10^{-3}	9.98×10^{-3}
	3	6.34×10^{-3}	1.27×10^{-2}	7.03×10^{-3}	1.41×10^{-2}
	4	4.65×10^{-3}	1.66×10^{-2}	5.15×10^{-3}	1.84×10^{-2}
	5	2.59×10^{-3}	2.06×10^{-2}	2.85×10^{-3}	2.29×10^{-2}
	6	1.79×10^{-4}	2.47×10^{-2}	1.50×10^{-4}	2.74×10^{-2}

TABLE XXV: Real and imaginary parts of the difference $\Delta\omega$ between QNMs of potentials V_{GD_3} and V_{RN_3} for $\alpha \in \{0.9, 1.0\}$.

-
- [1] Abbott B P *et al.* (LIGO Scientific, Virgo) 2016 *Phys. Rev. Lett.* **116** 221101 [Erratum: *Phys.Rev.Lett.* 121, 129902 (2018)] (*Preprint* 1602.03841)
- [2] Abbott B P *et al.* (LIGO Scientific, Virgo) 2019 *Phys. Rev. D* **100** 104036 (*Preprint* 1903.04467)
- [3] Ovalle J 2017 *Phys. Rev. D* **95** 104019 (*Preprint* 1704.05899)
- [4] Ovalle J 2019 *Phys. Lett. B* **788** 213–218 (*Preprint* 1812.03000)
- [5] Estrada M 2019 *Eur. Phys. J. C* **79** 918 (*Preprint* 1905.12129)

- [6] Gabbanelli L, Ovalle J, Sotomayor A, Stuchlik Z and Casadio R 2019 *Eur. Phys. J. C* **79** 486 (*Preprint* 1905.10162)
- [7] Leon P and Las Heras C 2023 *Eur. Phys. J. C* **83** 260
- [8] Ramos A, Arias C, Fuenmayor E and Contreras E 2021 *Eur. Phys. J. C* **81** 203 (*Preprint* 2103.05039)
- [9] Sharif M and Naseer T 2023 *Phys. Dark Univ.* **42** 101324 (*Preprint* 2310.00872)
- [10] Rincón A, Gabbanelli L, Contreras E and Tello-Ortiz F 2019 *Eur. Phys. J. C* **79** 873 (*Preprint* 1909.00500)
- [11] Morales E and Tello-Ortiz F 2018 *Eur. Phys. J. C* **78** 841 (*Preprint* 1808.01699)
- [12] Panotopoulos G and Rincón A 2018 *Eur. Phys. J. C* **78** 851 (*Preprint* 1810.08830)
- [13] Singh K N, Maurya S K, Jasim M K and Rahaman F 2019 *Eur. Phys. J. C* **79** 851
- [14] Jasim M K, Maurya S K, Khalid Jassim A, Mustafa G, Nag R and Saif Al Buwaiqi I 2023 *Phys. Scripta* **98** 045305
- [15] Gabbanelli L, Rincón A and Rubio C 2018 *Eur. Phys. J. C* **78** 370 (*Preprint* 1802.08000)
- [16] Pérez Graterol R 2018 *Eur. Phys. J. Plus* **133** 244
- [17] Heras C L and Leon P 2018 *Fortsch. Phys.* **66** 1800036 (*Preprint* 1804.06874)
- [18] Torres-Sánchez V A and Contreras E 2019 *Eur. Phys. J. C* **79** 829 (*Preprint* 1908.08194)
- [19] Hensh S and Stuchlík Z 2019 *Eur. Phys. J. C* **79** 834 (*Preprint* 1906.08368)
- [20] Contreras E, Rincón A and Bargueño P 2019 *Eur. Phys. J. C* **79** 216 (*Preprint* 1902.02033)
- [21] Tello-Ortiz F, Maurya S K and Bargueño P 2021 *Eur. Phys. J. C* **81** 426
- [22] Andrade J, Ortega K Y, Klínger W N R, Copa R C G, Medina S S C and Cruz J D 2023 *Eur. Phys. J. C* **83** 1085
- [23] Zubair M, Azmat H and Jameel H 2023 *Eur. Phys. J. C* **83** 905
- [24] Bamba K, Bhatti M Z, Yousaf Z and Shoukat Z 2023 *Eur. Phys. J. C* **83** 1033 (*Preprint* 2307.10399)
- [25] Maurya S K, Mustafa G, Ray S, Dayanandan B, Aziz A and Errehymy A 2023 *Phys. Dark Univ.* **42** 101284
- [26] Iqbal N, Amir M, Alshammari M, Mohammed W W and Ilyas M 2025 *Eur. Phys. J. C* **85** 428
- [27] Tello-Ortiz F, Bargueño P, Alvarez A and Contreras E 2023 *Fortsch. Phys.* **71** 2200170
- [28] Contreras E and Fuenmayor E 2021 *Phys. Rev. D* **103** 124065 (*Preprint* 2107.01140)
- [29] Sharif M and Majid A 2020 *Chin. J. Phys.* **68** 406–418
- [30] Meert P and da Rocha R 2021 *Nucl. Phys. B* **967** 115420 (*Preprint* 2006.02564)
- [31] da Rocha R and Tomaz A A 2019 *Eur. Phys. J. C* **79** 1035 (*Preprint* 1905.01548)
- [32] da Rocha R and Tomaz A A 2020 *Eur. Phys. J. C* **80** 857 (*Preprint* 2005.02980)
- [33] Estrada M, Crispim T M and Alencar G 2024 *Fortsch. Phys.* **2025** 2400220 (*Preprint* 2410.06189)
- [34] da Rocha R and Hoff da Silva J M 2014 *EPL* **107** 50001 (*Preprint* 1408.2402)
- [35] Cavalcanti R T, da Silva A G and da Rocha R 2016 *Class. Quant. Grav.* **33** 215007 (*Preprint* 1605.01271)

- [36] Ovalle J, Casadio R, Contreras E and Sotomayor A 2021 *Phys. Dark Univ.* **31** 100744 (*Preprint* 2006.06735)
- [37] Liang Y, Lyu X and Tao J 2024 *Commun. Theor. Phys.* **76** 085402
- [38] Avalos R, Bargueño P and Contreras E 2023 *Fortsch. Phys.* **2023** 2200171 (*Preprint* 2303.04119)
- [39] Zhang C M, Zhang M and Zou D C 2023 *Chin. Phys. C* **47** 015106 (*Preprint* 2208.06830)
- [40] Ditta A, Javed F, Maurya S K, Mustafa G and Atamurotov F 2023 *Phys. Dark Univ.* **42** 101345
- [41] Mansour N, Toghray T, El Boukili A, Benami A, Daoudia A K and Sedra M B 2024 *Int. J. Mod. Phys. A* **39** 2450151
- [42] Mahapatra S and Banerjee I 2023 *Phys. Dark Univ.* **39** 101172 (*Preprint* 2208.05796)
- [43] Albalahi A M, Yousaf Z, Ali A and Khan S 2024 *Eur. Phys. J. C* **84** 9
- [44] Naseer T 2024 *Eur. Phys. J. C* **84** 1256 (*Preprint* 2501.03690)
- [45] Maurya S K, Jasim M K, Errehymy A, Boshkayev K, Mustafa G and Dayanandan B 2024 *Phys. Dark Univ.* **46** 101665
- [46] Misyura M, Rincon A and Vertogradov V 2024 *Phys. Dark Univ.* **46** 101717 (*Preprint* 2405.05370)
- [47] Cavalcanti R T, de Paiva R C and da Rocha R 2022 *Eur. Phys. J. Plus* **137** 1185 (*Preprint* 2203.08740)
- [48] Yang Y, Liu D, Övgün A, Long Z W and Xu Z 2023 *Phys. Rev. D* **107** 064042 (*Preprint* 2203.11551)
- [49] Li Z 2023 *Phys. Lett. B* **841** 137902 (*Preprint* 2212.08112)
- [50] Cavalcanti R T, Alves K d S and Hoff da Silva J M 2022 *Universe* **8** 363 (*Preprint* 2207.03995)
- [51] Priyadarshinee S 2024 *Eur. Phys. J. Plus* **139** 258 (*Preprint* 2308.05719)
- [52] Rehman H and Abbas G 2023 *Chin. Phys. C* **47** 125106
- [53] Avalos R and Contreras E 2023 *Eur. Phys. J. C* **83** 155 (*Preprint* 2302.09148)
- [54] Al-Badawi A, Jha S K and Rahaman A 2024 *Eur. Phys. J. C* **84** 145
- [55] Tello-Ortiz F, Avalos R, Gómez-Leyton Y and Contreras E 2024 *Phys. Dark Univ.* **46** 101547
- [56] Abbott B P *et al.* (LIGO Scientific, Virgo) 2019 *Phys. Rev. Lett.* **123** 011102 (*Preprint* 1811.00364)
- [57] Will C M 2014 *Living Rev. Rel.* **17** 4 (*Preprint* 1403.7377)
- [58] Regge T and Wheeler J A 1957 *Phys. Rev.* **108** 1063–1069
- [59] Cardoso V and Pani P 2019 *Living Rev. Rel.* **22** 4 (*Preprint* 1904.05363)
- [60] Barack L, Cardoso V, Nissanke S, Sotiriou T P and Askar A 2019 *Class. Quant. Grav.* **36** 143001 (*Preprint* 1806.05195)
- [61] Richarte M G, Martins E L and Fabris J C 2022 *Phys. Rev. D* **105** 064043 (*Preprint* 2111.01595)
- [62] Pani P 2013 *Int. J. Mod. Phys. A* **28** 1340018 (*Preprint* 1305.6759)
- [63] Miranda A S, Ballon Bayona C A, Boschi-Filho H and Braga N R F 2009 *JHEP* **11** 119 (*Preprint* 0909.1790)
- [64] Lin K, Pavan A B, de Queiroz A R and Abdalla E 2025 *Phys. Rev. D* **111** 084076
- [65] Anacleto M A, Campos J A V, Brito F A and Passos E 2021 *Annals Phys.* **434** 168662 (*Preprint* 2108.04998)

- [66] Oliveira R, Dantas D M, Santos V and Almeida C A S 2019 *Class. Quant. Grav.* **36** 105013 (*Preprint* 1812.01798)
- [67] Rougemont R, Critelli R and Noronha J 2018 *Phys. Rev. D* **98** 034028 (*Preprint* 1804.00189)
- [68] Richartz M 2016 *Phys. Rev. D* **93** 064062 (*Preprint* 1509.04260)
- [69] Bishop N T and Rezzolla L 2016 *Living Rev. Rel.* **19** 2 (*Preprint* 1606.02532)
- [70] Kokkotas K D and Schmidt B G 1999 *Living Rev. Rel.* **2** 2 (*Preprint* gr-qc/9909058)
- [71] Nollert H P 1999 *Class. Quant. Grav.* **16** R159
- [72] Berti E, Cardoso V and Starinets A O 2009 *Class. Quant. Grav.* **26** 163001 (*Preprint* 0905.2975)
- [73] Konoplya R A and Zhidenko A 2011 *Rev. Mod. Phys.* **83** 793 (*Preprint* 1102.4014)
- [74] Rodrigues Jr W A, da Rocha R and Vaz Jr J 2005 *Int. J. Geom. Meth. Mod. Phys.* **2** 305 (*Preprint* math-ph/0501064)
- [75] Ovalle J, Linares F, Pasqua A and Sotomayor A 2013 *Class. Quant. Grav.* **30** 175019 (*Preprint* 1304.5995)
- [76] da Rocha R and Hoff da Silva J M 2012 *Phys. Rev. D* **85** 046009 (*Preprint* 1202.1256)
- [77] Abdalla M C B, Hoff da Silva J M and da Rocha R 2009 *Phys. Rev. D* **80** 046003 (*Preprint* 0907.1321)
- [78] Contreras E and Bargueño P 2018 *Eur. Phys. J. C* **78** 558 (*Preprint* 1805.10565)
- [79] Ovalle J, Casadio R, da Rocha R, Sotomayor A and Stuchlik Z 2018 *EPL* **124** 20004 (*Preprint* 1811.08559)
- [80] Carroll S M 2019 *Spacetime and geometry* (Cambridge University Press)
- [81] Maggiore M 2007 *Gravitational Waves. Vol. 1: Theory and Experiments* (Oxford University Press)
- [82] Ferrari V, Gualtieri L and Pani P 2020 *General Relativity and its Applications* (CRC Press)
- [83] Zerilli F J 1974 *Phys. Rev. D* **9** 860–868
- [84] Konoplya R A, Zhidenko A and Zinhailo A F 2019 *Class. Quant. Grav.* **36** 155002 (*Preprint* 1904.10333)
- [85] Konoplya R A 2018 *Phys. Lett. B* **784** 43–49 (*Preprint* 1805.04718)
- [86] Churilova M S, Konoplya R A and Zhidenko A 2020 *Phys. Lett. B* **802** 135207 (*Preprint* 1911.05246)
- [87] Rincón A and Panotopoulos G 2020 *Phys. Dark Univ.* **30** 100639 (*Preprint* 2006.11889)
- [88] Schutz B F and Will C M 1985 *Astrophys. J. Lett.* **291** L33–L36